Pergamon

Int. J. Solids Structures Vol. 33, No. 11, pp. 1619–1650, 1996

0020–7683/96 $15.00 + .00

0020–7683(95)00115–8

DISTURBED STATE CONSTITUTIVE MODELING BASED ON STRESS–STRAIN AND NONDESTRUCTIVE BEHAVIOR

CHANDRA S. DESAI and JANOS TOTH
Department of Civil Engineering and Engineering Mechanics, University of Arizona, Tucson, AZ 85721, U.S.A.

(*Received* 2 *November* 1994; *in revised form* 10 *May* 1995)

Abstract—The proposed disturbed state concept (DSC) is based on the idea that a deforming material element can be treated as a mixture of two constituent parts in the *relative intact* (RI) and *fully adjusted* (FA) states, referred to as reference states. During external loading, the material experiences internal changes in its microstructure due to a process of self-adjustment, and as a consequence, the initial RI state transforms continuously to the FA state. The self-adjustment process, which may involve relative motions of material particles that can lead to microcracking and damage or strengthening, can cause disturbances in the observed response with respect to the responses under the two reference states. Then, the observed response is expressed in terms of the responses for the RI and FA states that are determined from laboratory tests on material specimens. The DSC permits development of unified constitutive models that include, hierarchically, other previous continuum and damage models as special cases. Various aspects of the DSC are verified here with respect to laboratory behavior of two materials, a cemented sand and a ceramic composite. Some of the unique features of this study are that (1) the constitutive behavior and parameters can be obtained from the stress–strain-volume change behavior, and from the measurements of ultrasonic P-wave velocities, (2) correlations between mechanical and ultrasonic response can be established, (3) the concept can provide a description of the crack density, and (4) it can be simplified for predicting the remaining life of materials through definition of constitutive models and evaluation of design moduli affected by mechanical and environmental loading.

1. INTRODUCTION

Constitutive modelling and associated testing toward characterization of the mechanical response of solid materials and interfaces/joints have been subjects of considerable current research interest. This is because, unless realistic models for the material response are developed based on laboratory tests and properly validated, solutions of engineering problems in which they are used, whether closed-form or numerical, will have only limited validity! Theories of elasticity, plasticity, thermoplasticity, thermoviscoplasticity, continuum damage, micromechanics and endochronic are often used to develop constitutive models for engineering materials. The scope of these developments is wide, and it is not intended here to provide a detailed review; however, similarities and differences between the DSC and some of these models are discussed in Appendix 1. Only those works directly relevant to the proposed modeling approach, which is called the disturbed state concept (DSC), are referenced herein.

The idea of the DSC, in a simple form, was proposed in Desai (1974), and was subsequently generalized [Desai (1987, 1992), Desai and Ma (1992), Armaleh and Desai (1994), Katti and Desai (1995), Chia and Desai (1994)]. It is based on the assumption that the deforming material element is a mixture of material parts in two reference states, relative intact (RI) and fully adjusted (FA) states. Its observed behavior can then be expressed in terms of the behavior of material parts in the two reference states, through the disturbance function.

The objectives of this paper are:

(1) to present a description of the disturbed state concept for modeling the mechanical response of engineering materials together with a new procedure for defining the disturbance function, D, based on ultrasonic P-wave velocity measurements,

(2) to show that the velocity measurements together with stress–strain–volume response can lead to an alternative representation of the critical state that can be used to simulate the FA state,

(3) to calibrate and validate various aspects of the model with respect to test behavior of a cemented sand and a ceramic composite,

(4) to show that the disturbance based on velocity measurements can be used to evaluate crack density under loading, unloading, and reloading, and

(5) to indicate that the nondestructive velocity measurements can be used to develop the constitutive equations for the pre peak and post peak responses, and to obtain design moduli to define the remaining life of materials; the latter shows that a fundamental model can be simplified for practical applications.

2. DISTURBED STATE CONCEPT

The disturbed state concept (DSC) is based on the idea that the observed behavior of a material element can be expressed in terms of its behavior in two reference states: (1) relative intact (RI) and (2) fully adjusted (FA). At any stage during deformation under mechanical and/or environmental loadings, the material element is considered to be composed of the mixture of randomly disturbed material parts in the (RI) and (FA) states, Fig. 1. For example, as discussed subsequently, the RI state can be represented by using linear elastic, elastoplastic, or other appropriate models, and carries elastic and inelastic strains and associated stresses in the part that is assumed to behave as a continuum. The FA state can be simulated by using the critical state or other appropriate models, and can be associated with microcrack or pore growth, ultimately leading to failure. In the FA state, the material reaches a state at which the energy dissipation in it approaches an invariant level [Chia and Desai (1994), Basaran and Desai (1994)].

It is assumed that the applied forces cause disturbances or changes in the material's microstructure through *interaction* between the two parts. As a consequence, the initially (relative) intact material is modified continuously, through a process of *natural self-adjustment* or self-organization [Aifantis (1989), Bak and Chen (1991)] in its microstructure, and a part of it approaches the FA state. Self-adjustment implies that the material is capable of adjusting its internal structure to bring itself to effective configurations for responding to external forces; it can involve internal changes such as translational, rotational, and normal movements of the particles, and microcracking. During the transformation, particles in the

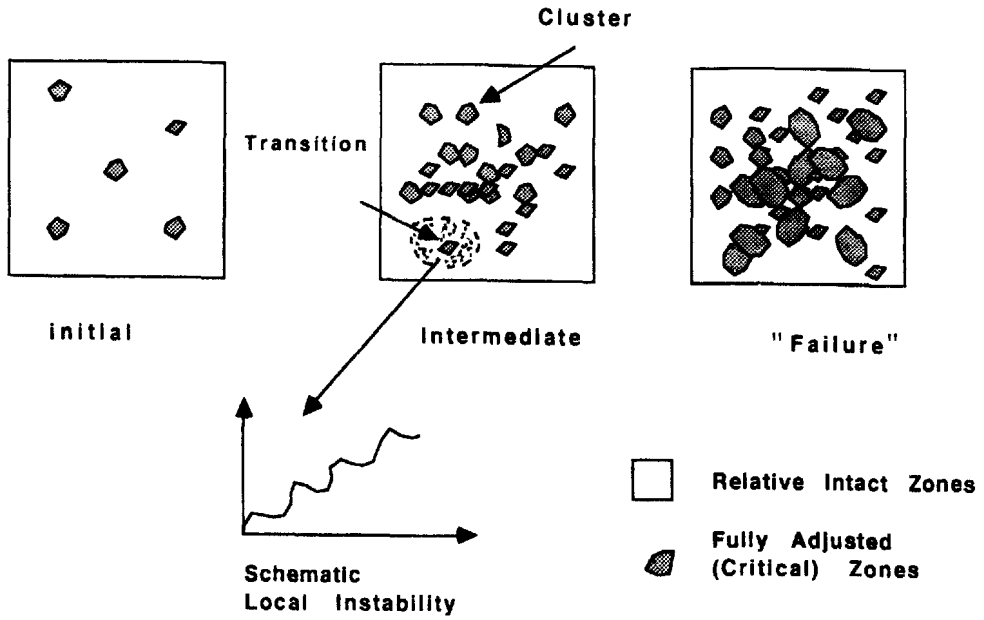

Fig. 1. Schematic of relative intact and fully adjusted clusters in DSC.

microstructure may experience local instability or transitions of its states, Fig. 1. At certain critical locations during deformation, the transitions may indicate threshold transitions involving significant or abrupt changes at states such as contractive to dilative volume change, peak stress, and initiation of residual stress conditions. This aspect is discussed later.

2.1. *Relative intact state*

The response of the material part that is at the RI state excludes the influence of factors under consideration that cause the disturbance; in this sense, it represents an "intact" state relative to the material state affected by the disturbance. For instance, response defined by the initial elastic moduli, Fig. 2(a), can be adopted as the RI state with respect to the observed nonlinear elastic behavior affected by factors such as microcracking (disturbance), which causes the deviation from the RI response. Here, $\bar{\sigma}$ and e denote measured stress and void ratio, respectively, and a, i and c denote observed, RI and FA responses, respectively. Note that the RI state can be dependent upon initial conditions such as the confining stress or mean pressure (σ_0) and density (ρ_0). In the limit, the ultimate or final RI state would correspond to the response at the maximum (σ_0) and (ρ_0); such final state is asymptotic

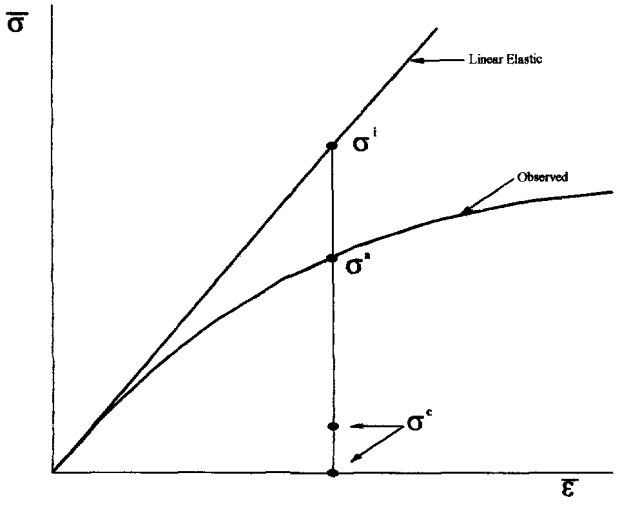

(a)

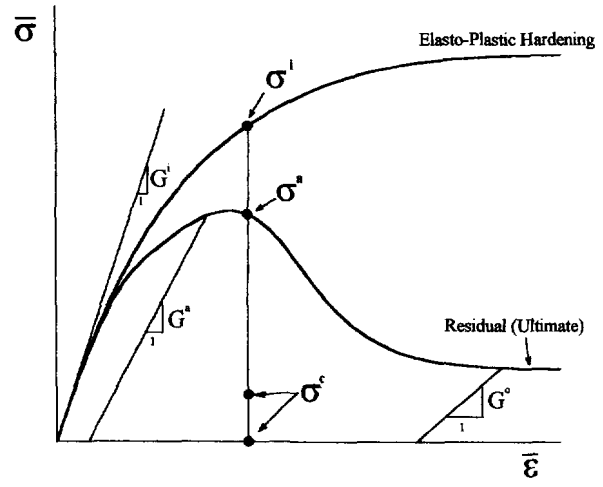

(b)

Fig. 2. Schematic of disturbance based on: (a) elastic behavior as RI state; (b) elastoplastic behavior as RI state; (c) volumetric (void ratio, e) response. (*Continued overleaf.*)

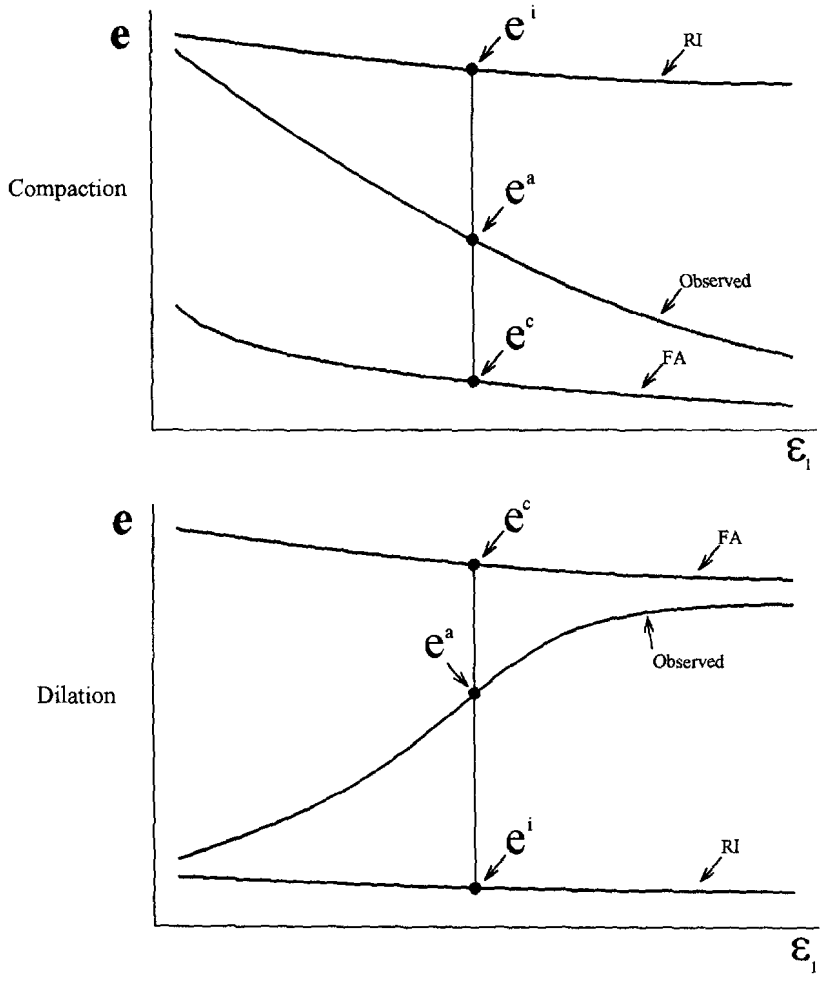

(c)

Fig. 2. *Continued.*

and may not be reached in practice. However, based on a series of tests under different values (maximum to minimum possible in the laboratory) of (σ_0) and (ρ_0), the moduli, e.g. the elastic modular E_i, can be defined as

$$E_i = E_i(\sigma_0, \rho_0) \tag{1}$$

where E_i is the (initial) elastic modulus; here, E_i^f will represent the asymptotic state.

Alternatively, the RI state can be defined on the basis of elastoplastic hardening behavior of the material part that does not experience disturbance due to microcracking and damage, Fig. 2(b). In that case, the RI can be defined by using the (δ_0) model in the hierarchical single surface (HISS) approach based on associative, isotropic hardening plasticity, Desai *et al.* (1986). It can also be represented by other models such as thermoplastic and thermoviscoplastic [Chia and Desai (1994)].

2.2. *Fully adjusted state*

The material part in the FA state can be considered to have reached an asymptotic state at which its structure reaches a condition in which its properties are different to those of the material in the RI state, and it may not be able to respond to the imposed shear and hydrostatic stresses as does the RI material. Various models can be adopted to characterize

this state; some of which are: (a) it possesses no strength, like ("void") in the continuum damage models [Kachanov (1958, 1986)], or (b) it possesses no strength in shear but can carry mean or hydrostatic stress [Frantziskonis and Desai (1987), Desai (1992)], like a "constrained liquid", or (c) it is at the critical state when it can continue to carry the shear under a given hydrostatic stress reached up to that state, and can experience shear strains without change in volume [Roscoe *et al.* (1958) and Desai (1992)], which may be treated as a "constrained liquid–solid" state. It is usually appropriate to define the FA state by employing the options (b) or (c) above, which are described later. This is because the material part in the FA state is surrounded by the RI material and is constrained. Hence, it is more appropriate to assign it a certain level of deformation and strength properties rather than considering it as a void without any strength.

2.3. *Disturbance function*

The observed behavior (a) is expressed in terms of the material's behavior at the RI (i) and FA (c) states by using the disturbance function, D; details are given subsequently.

2.4. *Analysis and comparisons*

Various aspects of the DSC such as free energy dissipation, nature of the tangent stiffness matrix involved in computation, and mesh dependence have been analyzed; they are described briefly in Appendix 1. The similarities and differences between the DSC and the classical damage model, and subsequent nonlocal damage theories including microcrack interactions, and the self-organized criticality theory, and reasons for the adoption of DSC, are discussed in Appendix 1.

3. LABORATORY TESTING

The model proposed herein is calibrated and validated with respect to test data on two materials, a cemented sand and a ceramic composite. Brief details of the tests and typical results are first presented below.

3.1. *Cemented sand*

Cubical specimens ($100 \times 100 \times 100$ mm) of cemented sand consisted of Leighton-Buzzard sand with 5% by weight of Burke stone (quick-setting cement) and 14% by weight of water. The specimens were cast in specially designed cubic molds, removed after 24 hours, and a thin coat of quick cement paste was applied on all the faces to ensure a smooth surface for a close greased connection to ultrasonic transducers, Fig. 3 [Jagannath *et al.* (1991), Desai *et al.* (1995)].

A cubical specimen was installed in the cavity of the multiaxial device in which 18-linear variable differential transformers (LVDTs), three on each face, allow measurements of induced (average) strains in the three principal directions. One ultrasonic transducer (0.5 MHz frequency) was installed on each of the six faces, Fig. 3, and allowed transmission of a P-wave in each of the three directions and measurements of the received waves at the three opposite sides. The cubical specimens were tested under hydrostatic (HC) and different compression and extension stress paths indicated in Fig. 3(b). In the latter, initial hydrostatic (confinement) stress $\sigma_0 = J_1/3$ was first applied and then the specimen was tested under different shear loadings. Two to three loading, unloading and reloading cycles were performed for each stress path test. During the cyclic loading, stresses and strains were recorded, as well as the ultrasonic results from which the velocities (V_x, V_y, and V_z) were evaluated. Details of the stress–strain test results are given in Jagannath *et al.* (1991) and Desai *et al.* (1995). It was observed that the cemented sand exhibits behavior that includes plastic or irreversible strains.

3.2. *Ceramic composite*

The ceramic composite is manufactured by using a special thermal process [Desai and Girdner (1992), Toth and Desai (1994), Toth (1994)]. Here, a mixture of a finely ground basaltic rock that simulates lunar soil or regolith and metal fibers (about 15% by weight

of stainless steel) is heated in a furnace, subjected to cycles of heating and cooling around the temperature of about 1100°C when the mixture melts or liquefies, and then it is cooled to room temperature. The resulting ceramic composite possesses desirable compressive, tensile, fracture and toughness properties for use in engineering construction (on the moon). Flat specimens of size $3.0 \times 6.0 \times 0.5$ inches ($7.6 \times 15.2 \times 1.3$ cm) are tested under tension and compression loading, unloading and reloading; they involved two tests each for the plain and fiber reinforced ceramic. The specimens are instrumented with strain gages at different locations, Fig. 4(a). A specially designed carriage system, which is installed in a MTS loading frame, permits movement of the transducers to different locations on the specimen, and measurements of ultrasonic velocities and attenuation of waves at different locations on the specimens, Fig. 4(b) [Tang *et al.* (1992), Toth (1994)].

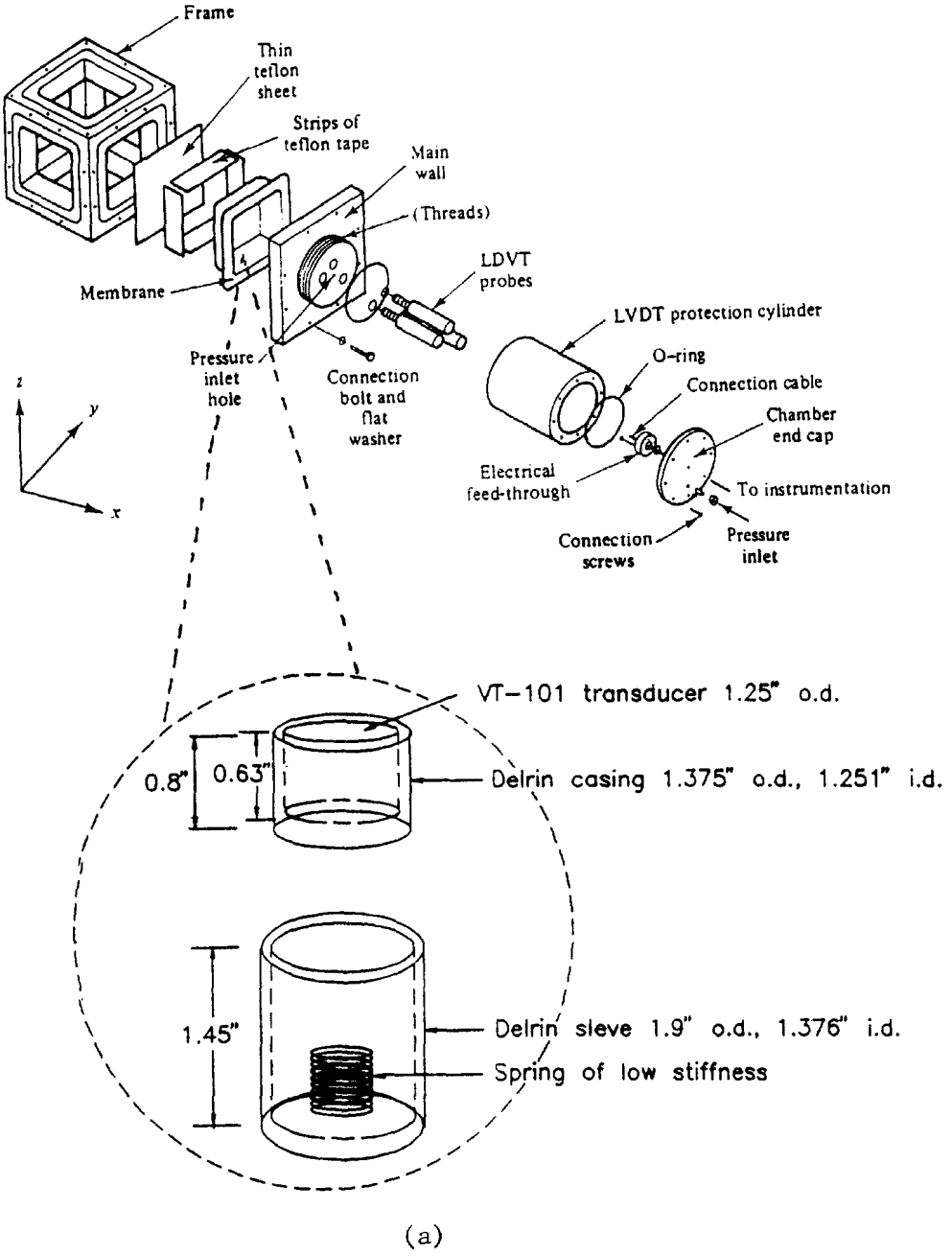

(a)

Fig. 3. Multiaxial testing of cemented sand: (a) device with ultrasonic transducers; (b) details of tests and stress paths. (*Continued opposite.*)

Test No.	Test Type	Stress Path	Figure
1	HC	Hydrostatic test with confining pressures up to 120 psi (830 kPa)	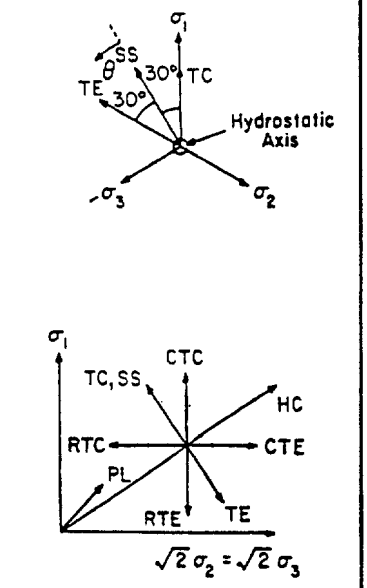
2	CTC20	CTC test with confining stress of 20 psi (138 kPa) with 1 psi (7 kPa) confining stress at various points along the stress path	
3	CTC30	CTC test with confining stress of 30 psi (207 kPa) with 1 psi (7 kPa) confining stress at various points along the stress path	
4	TE45	TE test with confining stress of 45 psi (310 kPa)	
5	TC30	TC test with confining stress of 30 psi (207 kPa)	
6	TE30	TE test with confining stress of 30 psi (207 kPa)	
7	CTC10	CTC test with confining stress of 10 psi (70 kPa)	

(b)

Fig. 3. *Continued.*

Loads, displacements and strains, and ultrasonic characteristics are recorded during loading, unloading and reloading. As the loading passed about 97% of the expected peak stress, it was stopped by fixing the position of the loading head. Then the measurements for about 10 points were recorded during the post peak softening region until the specimen failed.

3.3. *Test results*

The stress–strain test data and ultrasonic velocity measurements are utilized to develop the model and obtain correlations and validations herein. Typical test results derived from stress–strain data are described below.

Figures 5(a–d) show the results for the cemented sand in terms of J_1 vs $\sqrt{J_{2D}}$ (where J_1 is the first invariant of the stress tensor, σ_{ij}, and J_{2D} is the second invariant of the deviatoric stress tensor, S_{ij}), under different stress paths, Fig. 3(b), average ultrasonic velocity, $\bar{V} = (V_x + V_y + V_z)/3$ vs J_1 [where x, y and z denote three principal directions in the cubical specimen, Fig. 3(a), here z is the vertical direction], $\bar{V}^c$ vs $\ln(J_1/3p_a)$ (where $\bar{V}^c$ is the velocity in the FA or critical state and p_a is the atmospheric pressure), and void ratio e^c vs $\ln(J_1/3p_a)$, respectively. The void ratio, e, is defined as V_v/V_s, where $V_v = V_t - V_s$ is the volume of voids, $V_s = m\rho$ is the volume of solids, m is the mass, ρ is the density of solid particles, and V_t is the total volume of the specimen. Figure 6 shows results in terms of J_1 vs $\sqrt{J_{2D}}$ vs $\bar{V}$ for different stress paths. In Fig. 5(a), the critical state represents average curve through the state of stress at which the velocity reaches the critical invariant values, $\bar{V}^c$, Fig. 7. Figure 5(b) shows $\bar{V}$ vs J_1 for the HC test, and the average critical velocities ($\bar{V}^c$) corresponding to the asymptotic values near the end of tests. In Figs 5(c) and (d) are shown the average straight lines that represents critical values of $\bar{V}^c$ and e^c, respectively.

Figures 7(a and b) show plots of measured V_x, V_y, V_z, and $\bar{V}$ vs $\sqrt{J_{2D}}$ for a typical compression test (CTC 30), and extension test TE 45 for the cemented sand, respectively. Figure 7(c) shows typical results in terms of $\bar{V}$ vs $\sqrt{J_{2D}}$ for the ceramic fiber-composite. Here, the velocity at the end of the hydrostatic tests (at $\sqrt{J_{2D}} = 0$) for the multiaxial test

on the cemented sand represents initial velocity, $\bar{V}^i$, which indicates the influence of disturbance due to initial conditions. For the ceramic composite, the initial velocity represents effects of initial flaws and microcracking. It is assumed that in the beginning, that is, before any load was applied, the material specimen was in the RI state, and a value of velocity somewhat (about 10%) higher than the initial value can be treated as $\bar{V}^i$ for the RI state. For simplicity, an arbitrarily constant value of $\bar{V}^i$ for the RI state equal to 1175 m/s is adopted herein, Fig. 7(a,b), for the cemented sand, and 5665 m/s for the ceramic, Fig. 7(c). Here, $\bar{V}^a$ and $\bar{V}^c$ denote observed and critical velocities, respectively. It can be seen from Fig. 7 that as the material deforms, the average velocity appears to tend towards a constant critical value, $\bar{V}^c$, which is dependent on J_1. Further analysis is given later.

4. CONSTITUTIVE EQUATIONS

Details of the derivations for incremental observed stresses, $d\sigma_{ij}^a$ and strains, $d\varepsilon_{ij}^a$, in terms of the responses of the RI and FA parts are given by Desai (1992); only the equations are stated below. Based on the equilibrium of forces in the observed, RI and FA states and the disturbance function, D_σ, defined on the basis of stresses [subsequent eqn (8a)], the incremental observed stress tensor is given by

$$d\sigma_{ij}^a = (1-D_\sigma)\,d\sigma_{ij}^i + D_\sigma\,d\sigma_{ij}^c + dD_\sigma(\sigma_{ij}^c - \sigma_{ij}^i) \tag{2a}$$

or

$$d\sigma_{ij}^a = (1-D_\sigma)C_{ijkl}^i\varepsilon_{kl}^i + D_\sigma C_{ijkl}^c\,d\varepsilon_{kl}^c + dD_\sigma(\sigma_{ij}^c - \sigma_{ij}^i) \tag{2b}$$

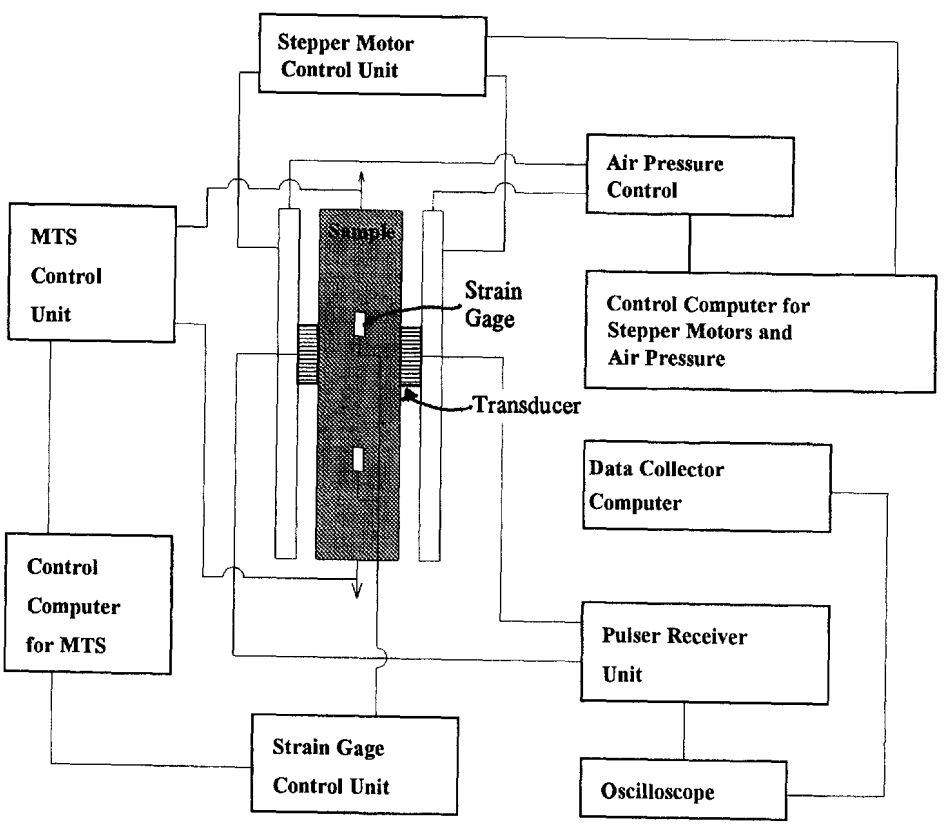

(a)

Fig. 4. Testing for ceramic: (a) specimen in MTS test setup; (b) carriage for moving ultrasonic transducers [Jagannath *et al.* (1991), Tang *et al.* (1992)]. (*Continued opposite.*)

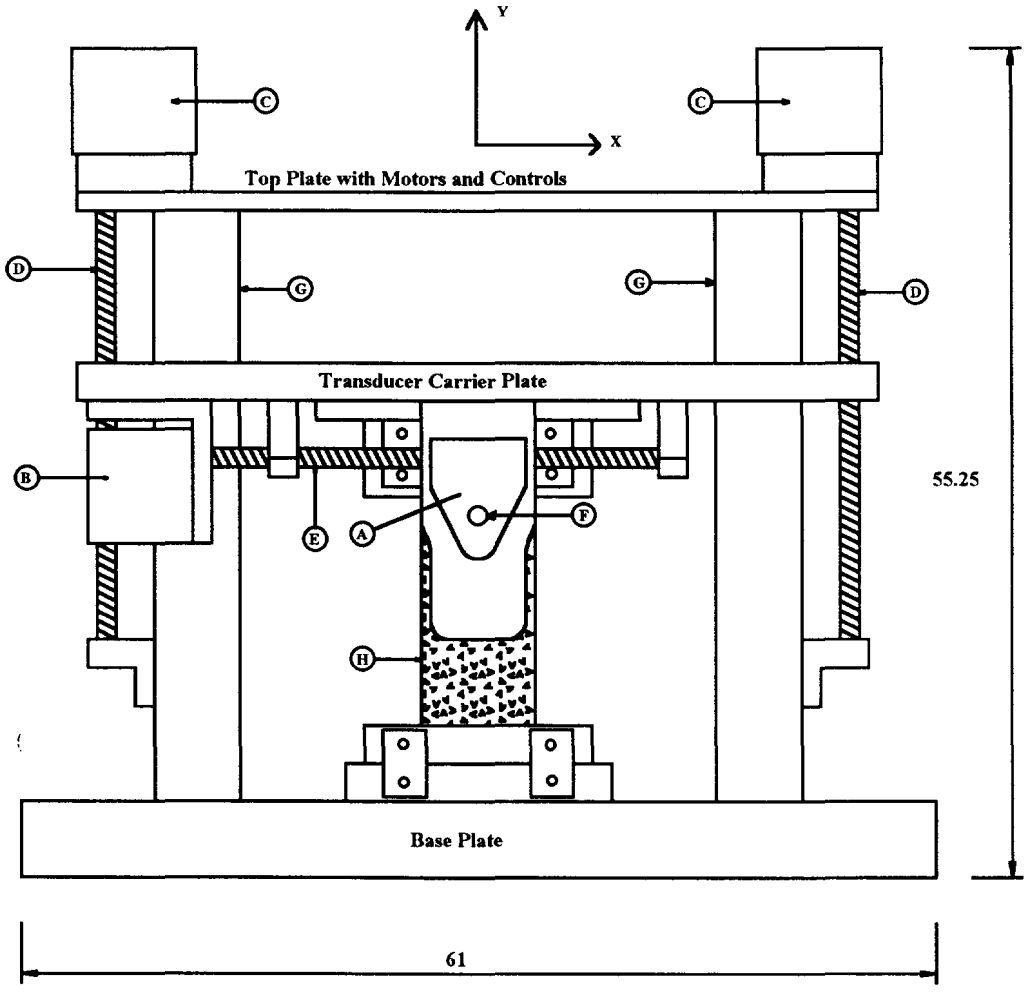

(b)

Fig. 4. *Continued.*

where C_{ijkl} is the fourth-order tensor related to the constitutive response, and superscripts a, i and c denote observed, RI and FA responses, respectively.

Considering the volumetric response and the disturbance function D_e [subsequent eqn 8(b)] based on void ratio, e, incremental observed strain tensor is given by

$$d\varepsilon_{ij}^a = dE_{ij}^a + D_e\, d\varepsilon_v^c \delta_{ij} + (1 - D_e)\, d\varepsilon_v^i \delta_{ij} + dD_e[(e^c - e^i)/(1 + e_0)]\delta_{ij} \tag{2c}$$

where ε_v is the volumetric strain, E_{ij}^a is the observed deviatoric strain tensor, δ_{ij} is the Kronecker delta, and e_0 is the initial void ratio; e is defined as the ratio of volume of voids to that of solids.

For the general formulation of the DSC, eqn (2) is implemented in finite element procedures (Appendix 1), and the solutions for stresses and strains are obtained using an iterative procedure. In other words, these strains and stresses above are interrelated, e.g. as

$$\varepsilon_{ij}^{i} = \varepsilon_{ij}^{i}(\varepsilon_{ij}^{a}, \sigma_{ij}^{a}, D) \tag{2d}$$

so that the iterated solution satisfies both the above equations for stresses and strains.

Equations (2a) and (2b) can be simplified significantly if certain assumptions are made. If it is assumed that the strains and mean pressure ($J_1/3$) are the same for the observed, RI and FA states, and the FA state carry only mean pressure, only one equation results as

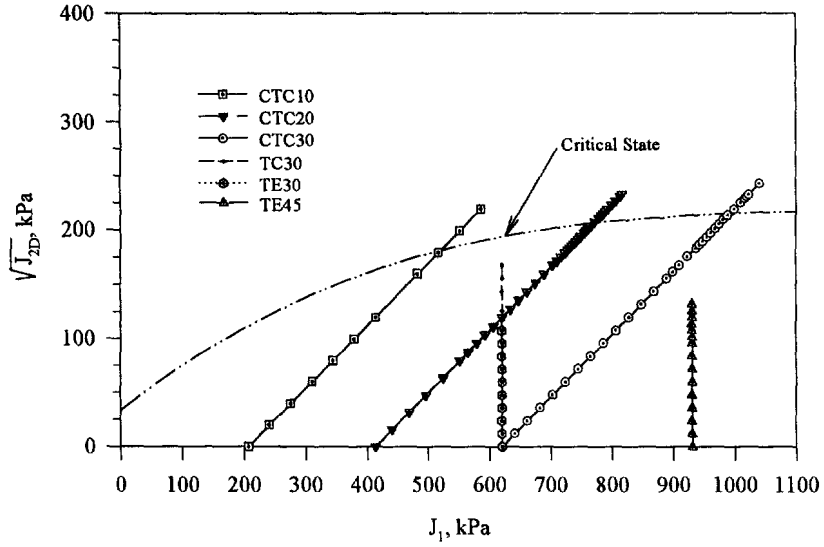

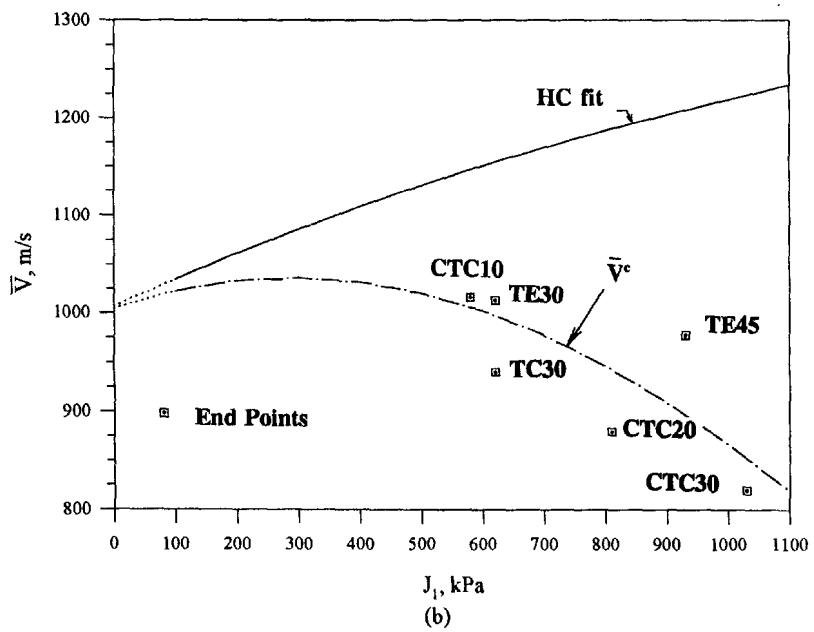

Fig. 5. Representation of test behavior of cemented sand: (a) J_1 vs $\sqrt{J_{2D}}$; (b) J_1 vs $\bar{V}$; (c) $\ln(J_1/3p_a)$ vs $\bar{V}^c$; (d) $\ln(J_1/3p_a)$ vs e^c. (*Continued opposite.*)

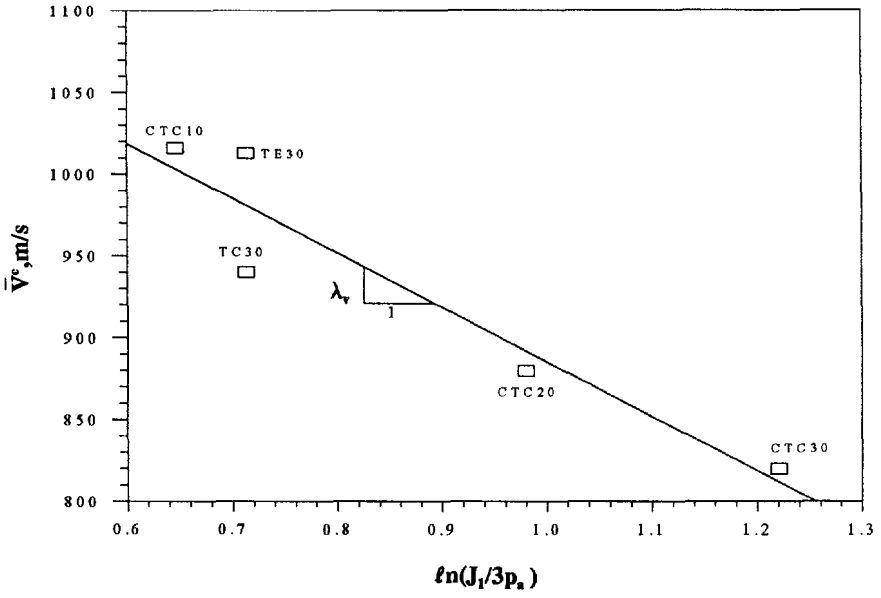

(c)

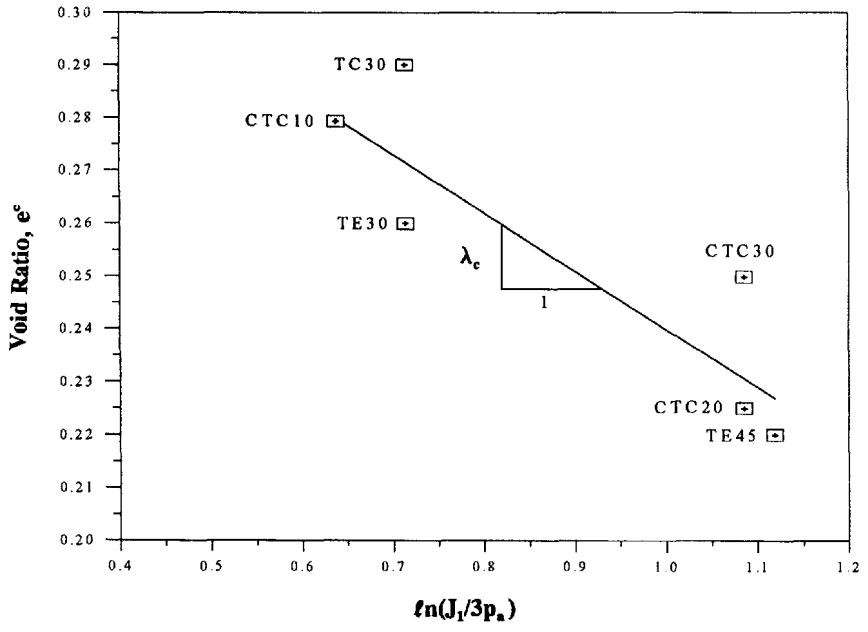

(d)

Fig. 5. *Continued.*

follows [Frantziskonis and Desai (1987)]:

$$d\sigma_{ij}^a = (1-D_\sigma)\, d\sigma_{ij}^i + \frac{D_\sigma}{3}\delta_{ij}\sigma_{kk}^i - dDS_{ij}^i \tag{3a}$$

where S_{ij} is the deviatoric stress tensor. Also, if it is further assumed that the material in the FA state does not carry any stress, eqn (3a) reduces to

$$d\sigma_{ij}^a = (1-D_\sigma)\, d\sigma_{ij}^i - dD_\sigma \sigma_{ij}^i \tag{3b}$$

which is the same as that in the classical damage and modified damage theories, e.g.

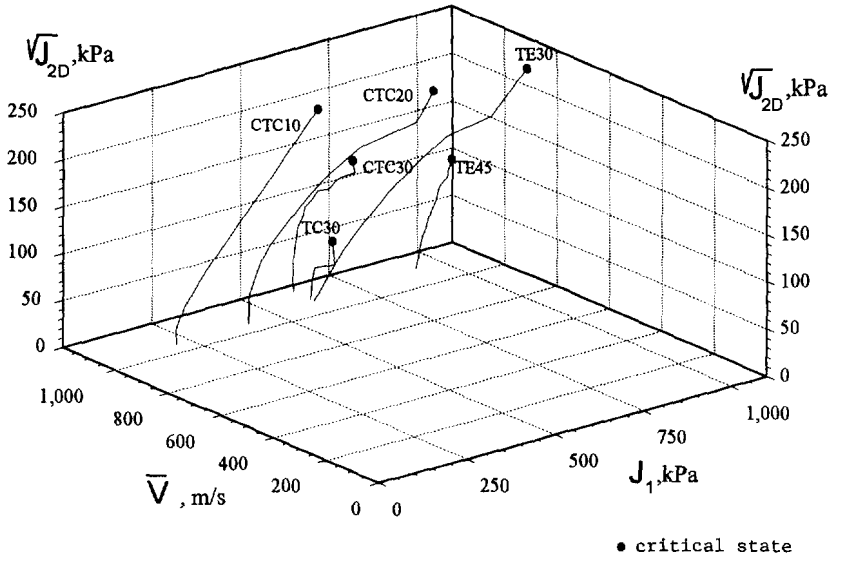

Fig. 6. Representation of behavior of cemented sand in three-dimensional J_1 vs $\sqrt{J_{2D}}$ vs $\bar{V}$ space.

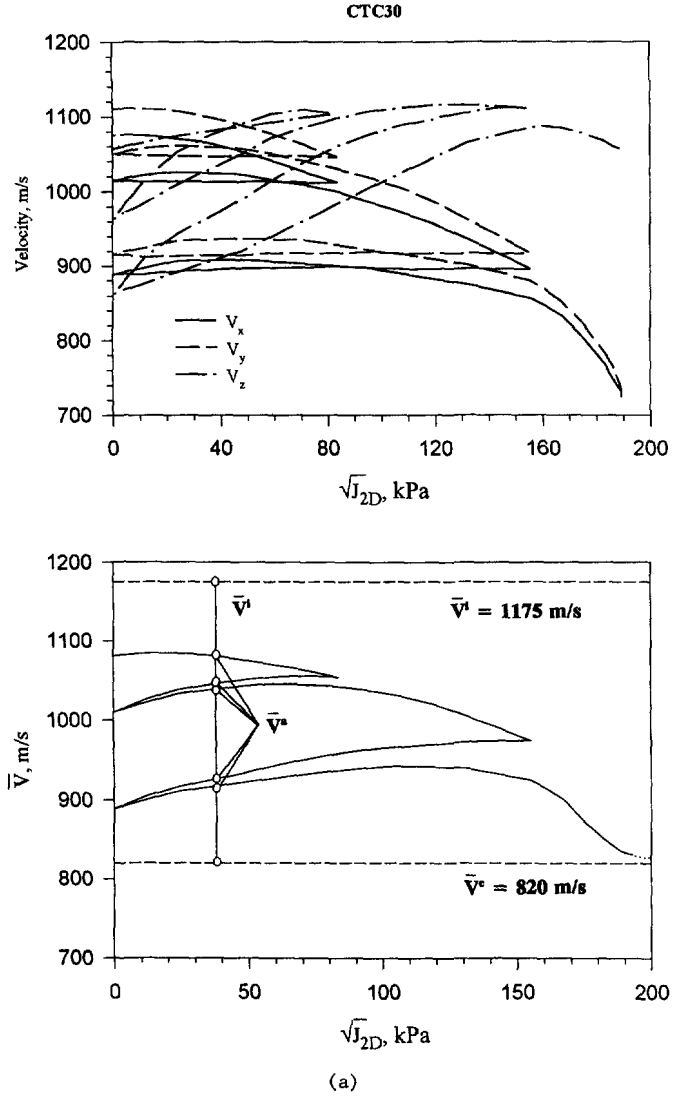

(a)

Fig. 7. Measured ultrasonic P-wave velocity components and average velocity: (a) CTC 30 test; (b) TE 45 test for cemented sand; (c) tensile test for fiber reinforced ceramic. (*Continued opposite.*)

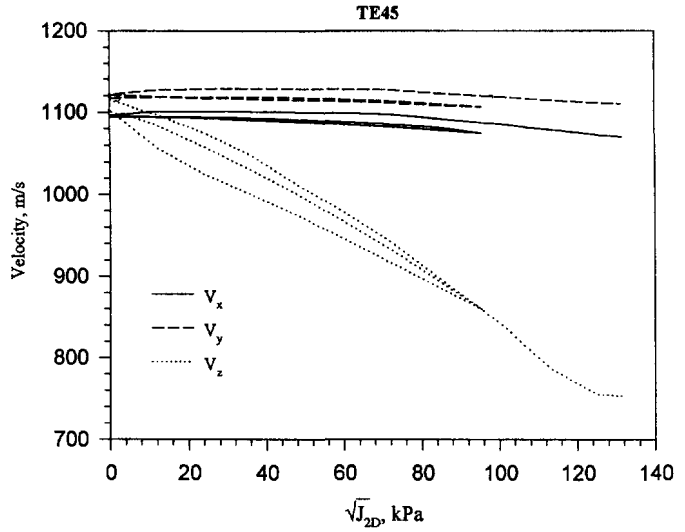

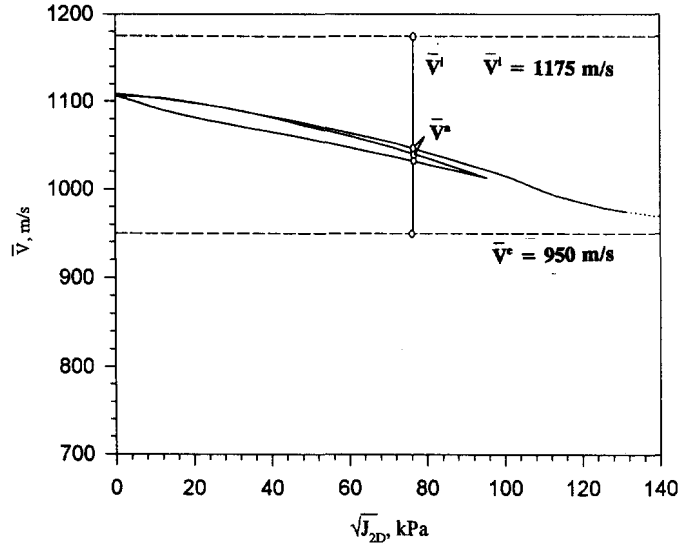

(b)

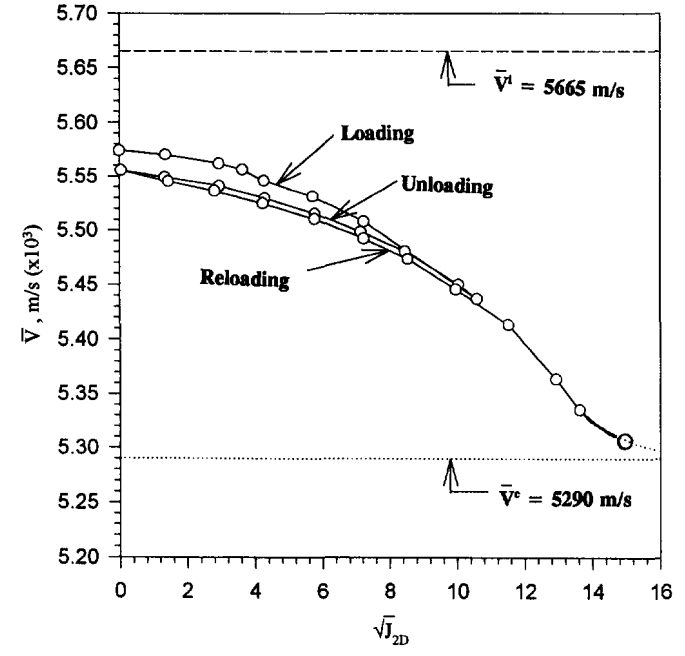

(c)

Fig. 7. *Continued.*

Kachanov (1958, 1986), Pijaudier-Cabot and Bazant (1987). Thus, it may be noted that the general DSC model, eqn (2a) and (2b), includes the classical damage formulation as a special case, and D_a in the specialized eqn (3b) is the same as the traditionally used damage parameter (ω); this aspect is discussed further in Appendix 1.

4.1. *Relative intact and fully adjusted states*

Constitutive equations for the relative intact state are expressed by writing $d\sigma_{ij}^i$ in eqn (3) as

$$d\sigma_{ij}^i = C_{ijkl}^i \, d\varepsilon_{kl}^i \tag{4}$$

where C_{ijkl}^i is the constitutive tensor for the (RI) state, which can be defined based on an appropriate theory such as linear elasticity and elasto-plasticity (associative hardening), Fig. 2b.

Depending upon the description of the FA state stated above, eqn (2) will be simplified accordingly. Since one of the main objectives here is to adopt the critical state to represent the FA state and to simulate it by its new representation using the (ultrasonic) velocities, its brief description is given herein. In this concept, under a given path of loading with the initial confinement ($\sigma_0 = J_1/3$), the material approaches the critical state at which it experiences shear strains at constant volume or void ratio under the same shear stress $\sqrt{J_{2D}}$ reached up to that state [Roscoe *et al.* (1958), Desai (1992)]. The behavior of the material at the critical state is defined based on the following relations:

$$\sqrt{J_{2D}^c} = \bar{m} J_1^c \tag{5a}$$

and

$$e^c = e_0^c - \lambda_e (J_1^c / 3p_a) \tag{5b}$$

where $\bar{m}$ is the (average) slope of the critical state line, Fig. 5(a), e_0^c is the value of e^c corresponding to $J_1 = 3p_a$, λ_c is the slope of the $\ln(J_1/3p_a)$ vs e^c plot, Fig. 5(c), and p_a is the atmospheric pressure constant which is used to nondimensionalize the stress. The value of e_0^c and λ_e for the cemented sand are found to be 0.27 and 0.11, respectively. When the FA state is represented by the critical state, eqns (5) are incorporated in eqn (2).

The idea of the critical state can be interpreted also in terms of ultrasonic (average) P-wave velocity, $\bar{V}$. Here, the deforming material under a given initial σ_0 approaches the critical state at which the velocity, $\bar{V}^c$, remains constant, like the void ratio in the classical critical state concept. Based on the laboratory tests (Section 3.0), the relation between the critical velocity $\bar{V}^c$ and mean pressure $J_1^c/3p_a$, analogous to eqn (5b), is obtained as

$$\bar{V}^c = \bar{V}_0^c - \lambda_v (J_1^c / 3p_a) \tag{6}$$

where $\bar{V}_0^c$ is the value of $\bar{V}^c$ corresponding to $J_1/3p_a$, and λ_v is the slope of $\ln(J_1/3p_a)$ vs $\bar{V}^c$ plot, Fig. 5(c). The value of $\bar{V}_0^c$ and λ_v for the cemented sand are found to be 1200 m/s and 334 m/s, respectively.

As shown in Fig. 6, under different stress paths with different initial confining pressures, σ_0, the cemented sand specimen approaches critical velocities. This behavior is similar to that presented in terms of q vs $\bar{p}$ vs e space in the classical critical state concept [Roscoe *et al.* (1958)] where $q = \sigma_1 - \sigma_3$, $\bar{p} = (\sigma_1 + \sigma_3)/2$, and σ_1 and σ_3 are the principal stresses.

For the cemented sand tested under multiaxial loading, the FA state is assumed to be the critical state defined by eqns (5). For the ceramic tested under uniaxial tensile loading, the FA is assumed to carry no tensile stress.

4.2. *Disturbance function*, D

The occurrence of significant microcracking and damage may initiate before the peak stress for materials such as soils (cemented sand herein), or mainly near and after the peak

for materials such as the ceramic composite. In order to cover a wide range of such behavior, a general and modified function for D, compared to the simplified form used previously [Desai (1992)], is now developed. It is given by [Weibull (1951), Lewis (1982)]

$$D = D_u\left[1 - \left\{1 + \left(\frac{\xi_D}{h}\right)^W\right\}^{-S}\right] \tag{7a}$$

where h, W and S are material parameters, and ξ_D is the trajectory of deviatoric plastic (or viscoplastic or thermoviscoplastic) strains E^p_{ij}:

$$\xi_D = \int (\mathrm{d}E^p_{ij}\,\mathrm{d}E^p_{ij})^{1/2}. \tag{7b}$$

Typical variation of D for different values of h are shown in Fig. 8 for $D_u = 1$; however, in practical material behavior $D_u < 1$, depending upon the experimental response. The expression in eqn (7a) is used to represent disturbance in terms of both the stress (D_σ) and velocity (D_v) below.

4.2.1. *Initial disturbance*, D_0. It is possible to incorporate initial disturbance, D_0, due to initial conditions such as sample preparation and manufacturing, initial flaws, discontinuities and anisotropy. Here, the anisotropy considered refers to that caused by factors such as specimen preparation in the laboratory; at this time, naturally anisotropic materials are not considered. For instance, if the stress–strain data under the initial hydrostatic stress (before the shear loading is applied) is available, the value of the initial plastic strain trajectory, ξ_{D_0}, can be evaluated. Then, the starting point for the shear loading will occur at D_0, Fig. 8, corresponding to ξ_{D_0}, eqn 7(a). Here, it is assumed that the initial conditions such as anisotropy cause shearing strains (under hydrostatic stress) and the disturbance function, D, is valid for that loading.

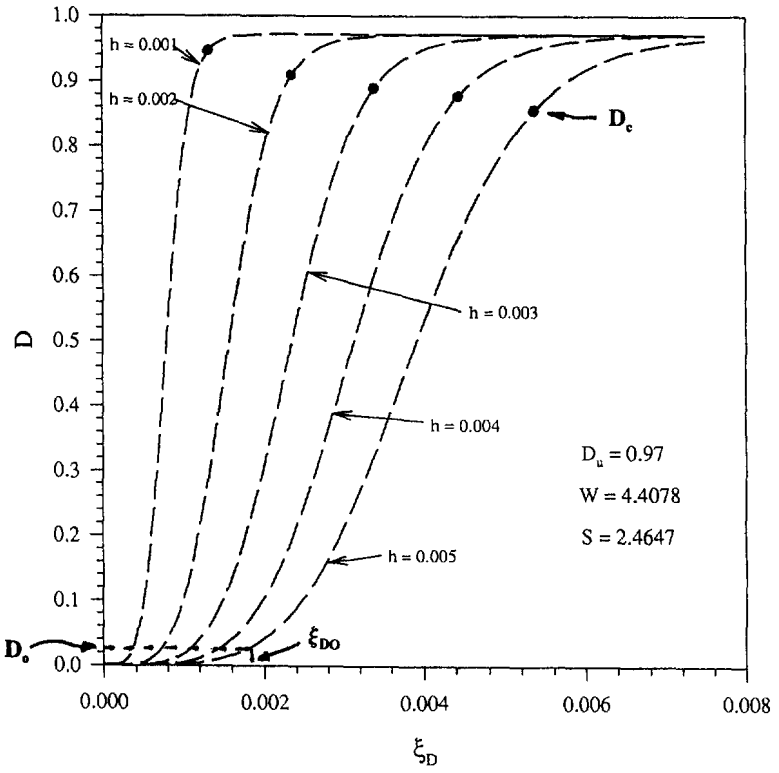

Fig. 8. Schematic of disturbance function D for different values of h.

As is explained below, the value of D_0 can also be found based on the measurements of ultrasonic velocities through the specimen before the loading is applied.

4.2.2. *Expressions for* D. The disturbance function, D, eqn (7a), and h, W and S, can be defined from the observed behavior. For example, D_σ, based on stress–strain behavior, Fig. 2(a,b), and D_e based on void ratio or volumetric behavior, Fig. 2(c), can be evaluated approximately from

$$D_\sigma = \frac{\bar{\sigma}^i - \bar{\sigma}^a}{\bar{\sigma}^i - \bar{\sigma}^c} \tag{8a}$$

and

$$D_e = \frac{e^i - e^a}{e^i - e^c}. \tag{8b}$$

Here, the overbar on σ denotes equivalent measured stresses such as the second invariant of the deviatoric stress tensor $\sqrt{J_{2D}}$, octahedral shear stress, τ_{oct} and stress difference, $\sigma_1 - \sigma_3$. These invariants are suggested for convenience because any other convenient measured stresses can be employed. The above definitions of D_σ and D_e have been used previously to develop the DSC constitutive equations for geologic and solder materials in semiconductor chip-substrate systems [Armaleh and Desai (1994), Katti and Desai (1994), Chia and Desai (1994)].

An alternative approach is proposed here for defining the disturbance function, D_v, from the average ultrasonic velocity measurements. Correlation between D_v and D_σ can then permit determination of D_σ from velocity measurements instead of stress–strain tests that can be expensive. Also, such a procedure can be extended to measurements of velocities *in situ* on existing structures, leading to the evaluation of the life of structures, design and rehabilitation; this is discussed later.

Based on the measurements of the average velocities $\bar{V}$, Fig. 7, the scalar isotropic disturbance, D_v, is defined as

$$D_v = \frac{\bar{V}^i - \bar{V}^a}{\bar{V}^i - \bar{V}^c} \tag{9}$$

where, as stated before, $\bar{V}^i = 1175$ m/s as adopted, $\bar{V}^c$ varies with the mean pressure, Fig. 5(c), for the cemented sand. For the ceramic under uniaxial tensile loading, approximate values of $\bar{V}^i = 5665$ m/s and $\bar{V}^c = 5290$ m/s are adopted.

It is possible to define directional values of D_i ($i = 1, 2, 3$) using eqn (9) corresponding to the values of the velocity components in the three (principal) directions x, y and z, Figs 7(a), (b). In that case, we can define a disturbance tensor with nonzero principal values by ignoring the coupling terms. The definition of such a disturbance tensor may be viewed in the same sense as the damage tensor defined by various investigators, e.g. Lubarda and Krajcinovic (1993). Such a description can provide a more general formulation of eqn (2). However, analysis toward existence and definition of such a tensorial nature of D would require additional research.

4.3. *Constitutive equations in DSC*

Introduction of material responses in the RI and FA states, eqns (4) and (5), respectively, and the disturbance function, D, eqn (7a), in eqn (2) leads to incremental constitutive equations as [see also eqns (A1–5b), Appendix 1]

$$\mathrm{d}\sigma_{ij}^a = C_{ijkl}^{DSC}\, \mathrm{d}\varepsilon_{kl}^i \tag{10}$$

where C_{ijkl}^{DSC} is the constitutive tensor which depends on the RI and FA responses and D. If

there is no disturbance, it specializes to that for the RI response which can be characterized as elastic, elastoplastic, etc. At this time when the RI state is assumed to be elastic, eqn (11) below, isotropy is assumed; however, it is possible to incorporate anisotropy in the elastic (RI) response. Irrespective of the model (elastic, elastoplastic, thermoviscoplastic, etc.) used for the RI state, the overall tensor $C_{ijkl}^{DSC}(D \neq 0)$ above includes anisotropic response during deformation; the effect of initial anisotropy (disturbance) can be incorporated as described in Section 4.2.1 above.

4.4 *Threshold transitions*

During deformation, the material experiences continuous transition from the RI to FA state. As indicated in Fig. 1, there may occur transition regions (shown by the dashed curve) in which the material transforms from the RI to the FA state; since the FA state itself is asymptotic, however, it is never reached. During the transition, the material (particles) may experience local instability, which is transmitted in a weighted sense, to the macro or global response. However, such a situation may not necessarily cause instability that results in collapse because the material continues to carry the applied load. On the other hand, at certain critical configurations of the deforming microstructure under transition, significant changes in the rate of transition (or disturbance) can occur, which are called *threshold transitions*.

More than one threshold transition may occur, depending upon the material and its characteristics. For instance, in the case of a (dense) granular material, they *may* occur at the stress state at which volume compaction changes to volume dilation, near the peak stress, and near or around the ultimate or residual state [Desai (1992)]. These states represent conditions when the changes in the microstructure are indicated by the changes in the rate of change in D, Fig. 8, as defined by the slope $(dD/D\xi_D)$ and curvature $(d^2D/D^2\xi_D)$. For instance, it is shown that the threshold transition state, marked D_c in Fig. 8, is related to the critical energy dissipation under cyclic loading at which fatigue failure occurs [Chia and Desai (1994)]. It is reported that instability causing liquefaction in saturated soils under cyclic loading occurs when the pore water pressure reaches the initial confining stress (σ_0) [Figuero *et al.* (1994)]; here, it is also shown that liquefaction (instability) occurs at the point when the rate of change in energy dissipation experiences a sudden change. Desai *et al.* (1995) have shown that the critical disturbance, D_c, Fig. 8, is also related to the point of critical energy dissipation at which liquefaction occurs. Additional investigations, including mathematical analysis and experiments, will be needed to relate these states to the observed material behavior, and to define initiation of microcracking and its propagation; these are in progress.

5. PARAMETERS AND VALIDATION

5.1. *Parameters*

As indicated earlier, the RI can be simulated using the linear elastic behavior, Fig. 2(a), or elasto-plastic hardening behavior, Fig. 2(b). In the case of the former, the values of the elastic moduli (Young's modulus E or shear modulus G, and Poisson's ratio ν) are required. Their values are found from (average) unloading slopes of stress–strain–volumetric responses if such tests are available. Alternatively, they can be obtained from ultrasonic velocity measurements, see Section 7 below. In the case of the elasto-plastic behavior, additional plasticity parameters γ, β, n, a, and η, are required; details of this model and parameters are given in Appendix 2. A number of previous studies have considered the elasto-plastic option: for interfaces and joints in rocks, Desai and Ma (1992); for cohesionless soil, Armaleh and Desai (1994); for cohesive soil, Katti and Desai (1994); and for solders in semiconductor chip-substrates, Chia and Desai (1994). Both possibilities are used herein.

For the linear elastic behavior, the values of D_σ are found using eqn (8a). For the elasto-plastic model, the relevant parameters are first found based on the early loading–unloading–reloading (pre peak) response, and the values of $\bar{\sigma}^i$ in eqn (8a) are then found by integrating the following equations:

$$\{d\sigma^i\} = [C^{epi}]\{d\varepsilon^i\} \tag{11}$$

where $[C^{epi}]$ is the elasto-plastic constitutive matrix, and $\{d\sigma^i\}$ and $\{d\varepsilon^i\}$ are the incremental stress and strain vectors, respectively, for the RI state.

The values of ξ_D at different points on the stress–strain curves are found using eqn (7b) and the corresponding values of D_σ are found using eqn (8a). Then, the values of parameters h, W and S are found by writing eqn (7a) as

$$\ln\left(\frac{D}{1-D}\right) = W \ln \xi_D - W \ln h. \tag{12}$$

In the plot of ξ_D vs $\ln[D/(1-D)]$ for a given value of S, W is related to the slope of the (average) line, and h to the intercept along the ordinate, which yields the value of ξ_D at the inflexion point along D, Fig. 8. Parameter S is related to the symmetry of the curve; for $S = 1$, the curve, Fig. 8, is symmetric. With estimated initial values of S ($= 1$) and h (approximately equal to ξ_D at the inflexion point), eqn (11) is solved iteratively to find the values of h, W and S.

Cemented sand. The values of h, W and S for D_σ for (multiaxial) tests under different σ_0 for the cemented sand are obtained assuming linear elastic RI state response; they are listed in Table 1. For D_v, the values of h_v, W_v and S_v were found based on eqn (9) and results such as those in Fig. 7, and by using eqn (12); they are also listed in Table 1.

It was found that the parameter h was essentially constant ($= 0.007$) with σ_0 and the same for both D_σ and D_v, while W and S were found to be approximate linear functions of σ_0 as

$$W = Z_w + A_w(\sigma_0/p_a)$$
$$S = Z_s + A_s(\sigma_0/p_a) \tag{13}$$

where Z and A are constants that are obtained by using tests under different stress paths, Fig. 3(b).

Ceramic. Since the tests are performed under uniaxial stress, the parameters h, W, S are independent of σ_0. Furthermore, for the material tested, their average values were found to be essentially constant for plain and fiber reinforced ceramic: for D_σ: $h_\sigma = 0.003$, $W_\sigma = 4.53$, $S_\sigma = 2.03$; and for D_v: $h_\sigma = 0.006$, $W_\sigma = 1.06$, $S_\sigma = 12.00$.

5.2. *Validations*

The disturbance functions D_σ and D_v are evaluated from test data for the cemented sand and the ceramic, and are compared with the predictions obtained by using eqn (7a) [Toth (1994)]. Here, predictions are obtained by using the computed (above) material parameters with four options: (a) based on specific test itself, (b) based on the CTC tests,

Table 1. Parameters h, W and S for cemented sand

	Parameters for D_σ			Parameters for D_v		
Test	h_σ	W_σ	S_σ	h_v	W_v	S_v
CTC 10		1.212	0.496		0.920	0.482
CTC 20		1.294	0.520		1.233	0.713
CTC 30	0.007	1.433	0.633	0.007	1.346	0.961
TC 30		1.195	0.589		1.165	1.050
TE 30		1.285	0.642		1.105	0.860
TE 45		1.395	0.697		1.246	0.986
Average	0.007	1.30	0.60	0.007	1.17	0.84

(c) based on all tests and (d) simple averages from all tests, Table 1. As expected, predictions with parameters based on the test itself yielded the best comparisons. However, predictions from the other three options also provided satisfactory comparisons. Thus, use of parameters from standard CTC tests can be used to simulate disturbance for all significant stress paths. The constitutive equations, eqns (10), are used to predict the laboratory behavior of the cemented sand and the plain and composite ceramic. Typical comparisons between predictions and laboratory test results are presented below.

5.2.1. *Prediction of stress–strain response.* The observed stress–strain responses of the cemented sand and plain and fiber reinforced ceramic specimens are predicted by integrating constitutive eqns (10) for the multiaxial or uniaxial stress loading, respectively; here, D_σ based on both linear elastic and elastoplastic responses for the RI states are considered, Fig. 2. For the cemented sand, the RI material is simulated as linear elastic and the FA material using the critical state, eqns (5). For the ceramic, the RI material is simulated as linear elastic or elasto-plastic, and the FA material is assumed to carry no tensile stress.

For each case, two ceramic specimens were considered. Then, in order to show the validity of the model, predictions for the first specimen test were obtained by using parameters from that specific test, and also by using parameters from the test on the second specimen, and vice versa. Thus, validation for independent tests was obtained. It was found that the model provided satisfactory predictions; typical results for the fiber reinforced ceramic are shown in Fig. (9). Figure 9(a) shows comparisons between observed response and computed responses based on linear elastic and elastoplastic RI states for the first specimen using parameters from the second specimen under *tension* loading, while Fig. 9(b) shows results for fiber-reinforced specimen 2 under *compression* loading using parameters from specimen 3. These results indicate that for this material, characterization of the RI state using both linear elastic and elastoplastic models provides satisfactory predictions.

Figure 10 shows comparisons between predictions and test data for stress–strain and volumetric behavior for typical extension (TE45), Fig. 3(b), test. It can be seen that the model provides satisfactory predictions.

6. CORRELATIONS

One of the objectives herein is to show that the ultrasonic velocity data can be used to define the constitutive relations and to assess the remaining life of materials. For instance, if the linear elastic behavior can be used, only limited stress–strain tests need to be performed to define the RI state. The FA state, as defined by the critical state concept and the disturbance function D_σ, can be found based on the velocity measurements. These aspects are discussed below only for the case of the cemented sand.

6.1. *Fully adjusted-critical state*

The value of $\bar{m}$ in eqn (5a) can be estimated approximately based on the stress at the critical state under compression stress paths with three initial σ_o. Once $\bar{V}_o^c$ in eqn (6) is established from velocity measurements, eqn (5b), required in the constitutive equation can be defined from the values of e_o^c and λ_e, and $\bar{V}_o^c$ and λ_v as

$$\bar{V}_0^c = (1200/0.27)e_0^c = 4450e_0^c \text{ m/s};$$
$$\lambda_v = (334/0.11)\lambda_e = 3040\lambda_e \text{ m/s}. \tag{14a}$$

In order to obtain D_σ from D_v, correlations between the parameters h_σ, W_σ, S_σ and h_v, W_v and S_v can be established based on the computed parameters, h, W and S. For instance, such linear relations are obtained for W_σ and S_σ (while h_σ is essentially constant) as

$$h_\sigma = h_v \simeq 0.007$$
$$W_\sigma = \bar{Z}_W + \bar{A}_W \cdot W_v$$

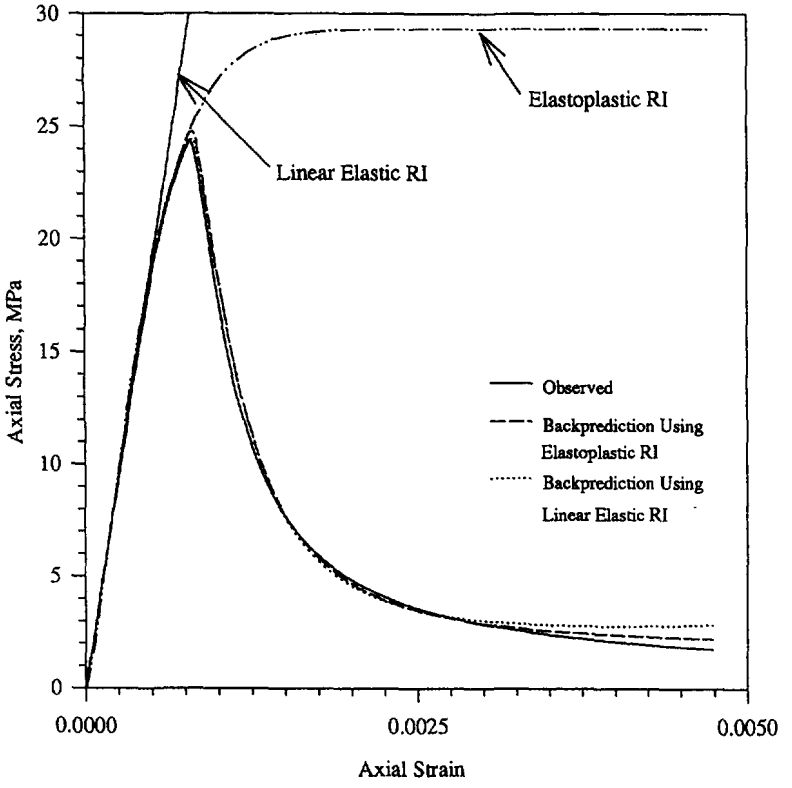

(a)

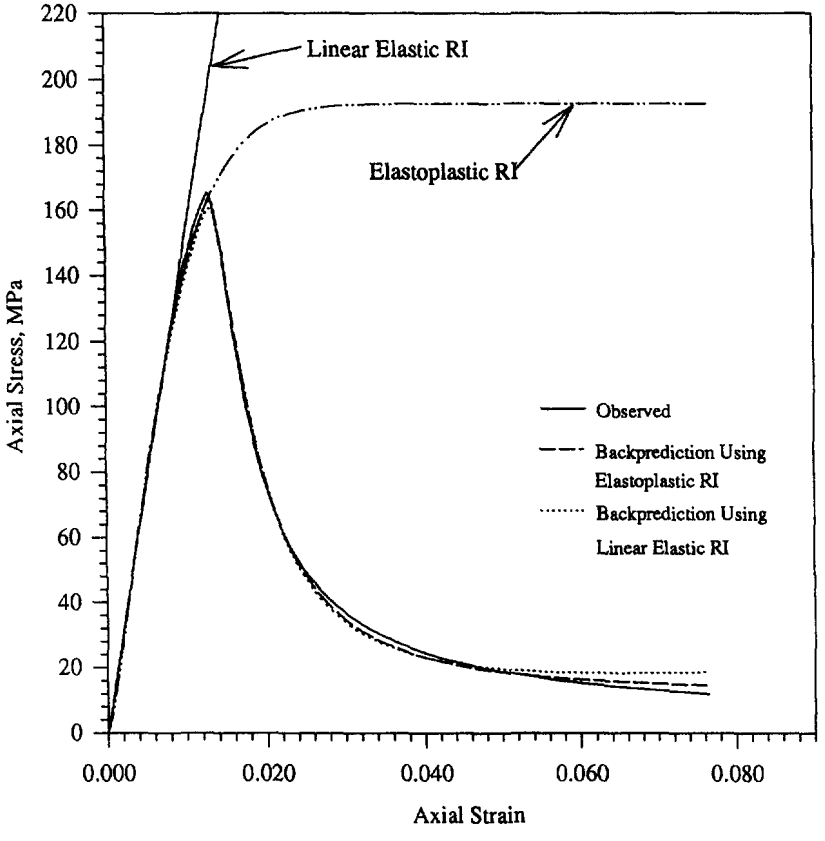

(b)

Fig. 9. Comparisons between predictions and test data for stress–strain response for ceramic (a) for tension fiber reinforced test 1 with parameters from test 2; (b) for compression fiber reinforced test 2 with parameters from test 3.

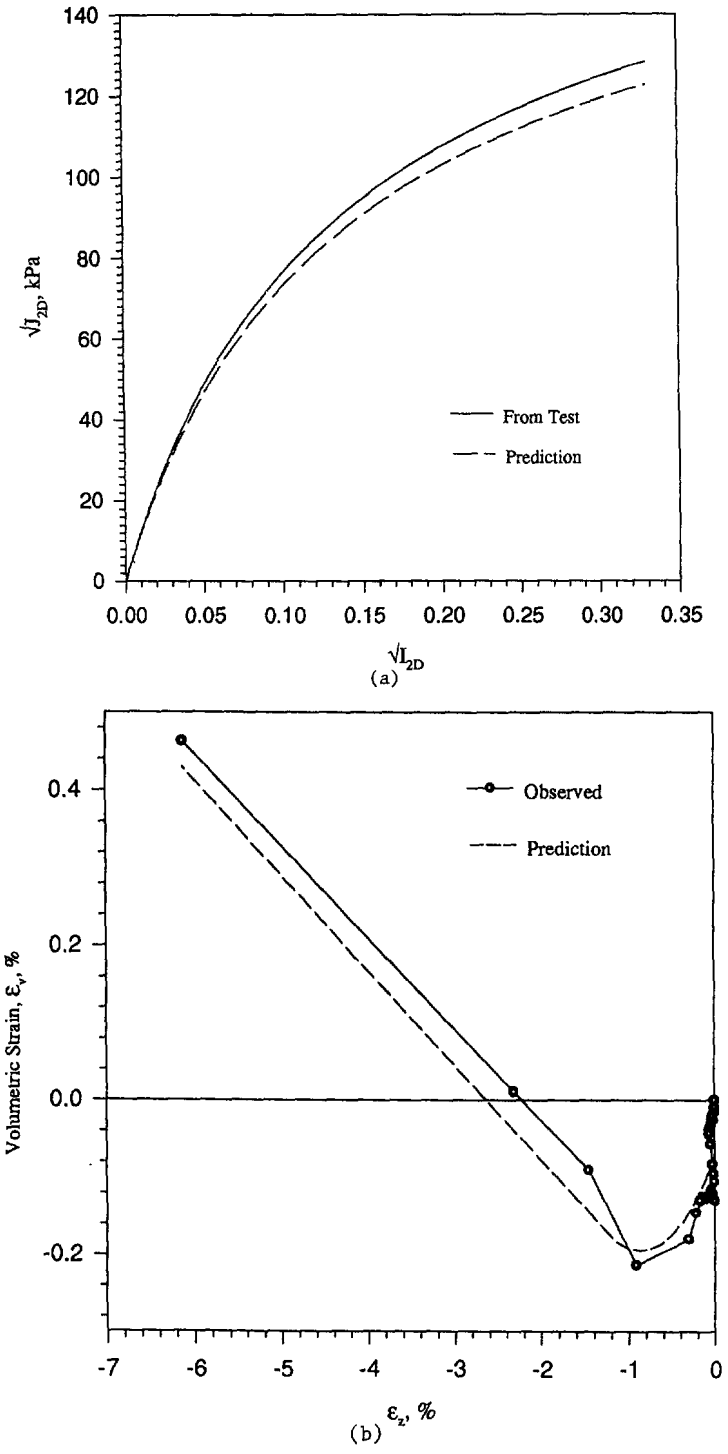

Fig. 10. Comparison between observed and predicted behavior for cemented sand–TE 45 test: (a) stress–strain; (b) volumetric.

$$S_\sigma = \bar{Z}_S + \bar{A}_S \cdot S_v. \tag{14b}$$

The values of the constants $\bar{Z}$ and $\bar{A}$ were obtained based on all the six tests and only the three CTC tests, Table 1. Thus, the constants for D_v from velocity measurements can be used to evaluate those for D_σ. Then, D_σ can be found using eqn (7a). Figure 11 shows the relation between D_σ and D_v for a typical CTC 30 test. Here, h_σ, W_σ, S_σ, eqn (14b), were

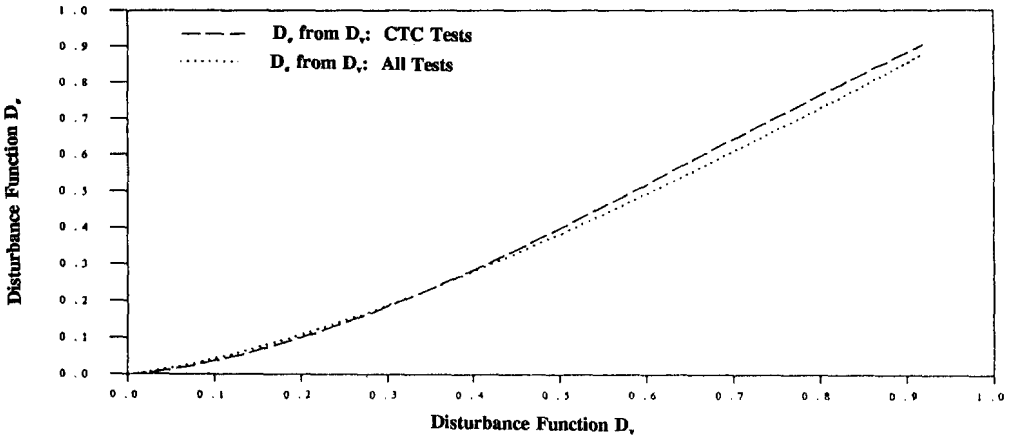

Fig. 11. Relation between D_σ and D_v

evaluated based on h_v, W_v and S_v from CTC tests and all tests. Then, the values of h_σ, W_σ and S_σ were used in eqn (7a) to evaluate D_σ.

7. OTHER APPLICATIONS

The DSC can be applied to model the cyclic time dependent behavior of materials including thermoviscoplastic characteristics and time dependent fatigue and degradation. It is also extended for the characterization of the behavior of interfaces and joints. In view of space limitations, these aspects are not detailed herein; they are presented in Desai and Ma (1992), Desai (1994) and Chia and Desai (1994). However, brief descriptions of the potential use of the DSC for the evaluation of constitutive models, remaining life of materials and for computation of crack density are presented below.

7.1. *Remaining life of materials*

As discussed in the above section, the constitutive equations for the entire stress–strain response under mechanical and environmental loading can be obtained from velocity measurements and limited stress–strain tests. Thus, the constitutive models can be obtained to define the current state and remaining life of materials in existing structures. Indeed, the correlation between functions needs to be first determined from laboratory and/or field tests, in which tests are performed at various stages during mechanical and environmental loading.

As indicated earlier, the elastic moduli can be derived based on the DSC. An example is given below. Consider the special form of eqn (3a) for the shear stress increment $d\sigma_{12}^a$:

$$d\sigma_{12}^a = (1-D_\sigma)[G^i\, d\varepsilon_{12}^i] + D_\sigma[G^c\, d\varepsilon_{12}^c] \tag{15a}$$

where G denotes the shear modulus. Now, if it is assumed that the observed RI and FA strains are compatible, that is, $d\varepsilon_{12}^a = d\varepsilon_{12}^i = d\varepsilon_{12}^c$, and if the FA state is assumed to carry no shear stress, that is, $G^c = 0$, eqn (15a) reduces to

$$d\sigma_{12}^a = (1-D_\sigma)G^i\, d\varepsilon_{12}^a \tag{15b}$$

which leads to the expression for (degrading) observed shear modulus, G_a, Fig. 2(b), in which $\bar{\sigma} = \tau_{oct}$ and $\bar{\varepsilon} = \gamma_{oct}$,

$$G^a = (1 - D_\sigma) \cdot G^i. \tag{15c}$$

If $\bar{\sigma} = \sigma_1 - \sigma_3$ and $\bar{\varepsilon} = \varepsilon_1$, relation for the Young's modulus E^a can be expressed as

$$E^a = (1 - \bar{D}_\sigma) E^i \tag{15d}$$

where $\bar{D}_\sigma$ is disturbance relevant to $(\sigma_1 - \sigma_3)$ vs ε_1 response.

The value of D_σ in eqn (7a) can be found from the velocity based disturbance parameters using eqn (14). Additional research will be needed for other material (design) parameters. However, this aspect could have potential applications in the rehabilitation of existing infrastructure problems.

7.2. *Evaluation of microcrack density*, C_d

The DSC and the knowledge of D can be used to evaluate the microcrack density, C_d, in deforming materials. A material specimen subjected to loading, unloading and reloading can experience initiation, propagation, opening, and coalescence of microcracks. This process is dependent on the initial conditions, stress paths, and such other factors as volume compaction and increase (dilation). Existence of the randomly disturbed microcracks can also lead to induced anisotropy [Jagannath *et al.* (1991), Desai *et al.* (1995)]. It is shown below that the ultrasonic velocities and the disturbance function, D_v, can permit description and definition of microcracking.

For this purpose, the equation below presented by Hudson (1981) and Sayers *et al.* (1990) is used. Here, it is assumed that the mean crack shape of randomly disturbed cracks is circular and the wavelengths of elastic waves are large compared with the size of cracks and with their separation distances, so that the mean over the statistical ensemble can be used to predict properties of a single sample. The equation for crack density is given by

$$C_d = \frac{\dfrac{15(1-\nu_0)}{2(1-2\nu_0)}\left(1 - \dfrac{V^{*2}}{V_0^2}\right)}{\left(2U_{11} + \dfrac{3 - 2\nu_0 + 7\nu_0^2}{(1-2\nu_0)^2} \cdot U_{33}\right)} \tag{16a}$$

$$= \Omega\left(1 - \frac{V^{*2}}{V_0^2}\right) \tag{16b}$$

where $U_{11} = 16(1-\nu_0)/3(2-\nu_0)$, $U_{33} = 8(1-\nu_0)/3$, ν_0 and V_0 are the Poisson's ratio, and P-wave velocity in the RI material and V^* is the observed root mean square P-wave velocity. Here, $C_d = na^3$, where n is the open cracks per unit volume, and a is the mean dimension (radius) of cracks [Hudson (1981)].

For the cemented sand, the Poisson's ratio is found to be about 0.35. Using this value, Ω is found to be 0.725. For the ceramic, average value of ν was found to be 0.24, and hence, $\Omega = 0.685$. Now, by considering V^* as $\bar{V}^a$, and V_0 as $\bar{V}^i$ in eqn (9) for D_v, eqn (16) can be expressed as

$$C_d = \Omega\left[1 - \frac{(V^i - D_v V^i + D_v \bar{V}^c)^2}{(\bar{V}^i)^2}\right]. \tag{17}$$

A plot of C_d vs $\sqrt{J_{2D}}$ for a typical test (CTC 30) for the cemented sand is shown in

Fig. 12(a), for the loading–unloading and reloading responses. A corresponding plot of D_v vs $\sqrt{J_{2D}}$ is shown in Fig. 12(b). It can be seen, as is evident from the relation in eqn (17), that the disturbance function based on the P-wave velocity shows similar trends. During the monotonic or virgin loading, both increase. During unloading, as the load is removed, the cracks may experience opening, and C_d generally increases; similarly, as the observed velocity decreases, Fig. 7, D also increases. During reloading, the values of C_d and D_v decrease due to coalescence of cracks. Then, after the end of reloading and during subsequent virgin loading, they both increase. Note that in the CTC test $\sigma_1 > \sigma_2 (= \sigma_3)$; hence, when unloading occurs, σ_1 decreases while $\sigma_2 = \sigma_3$.

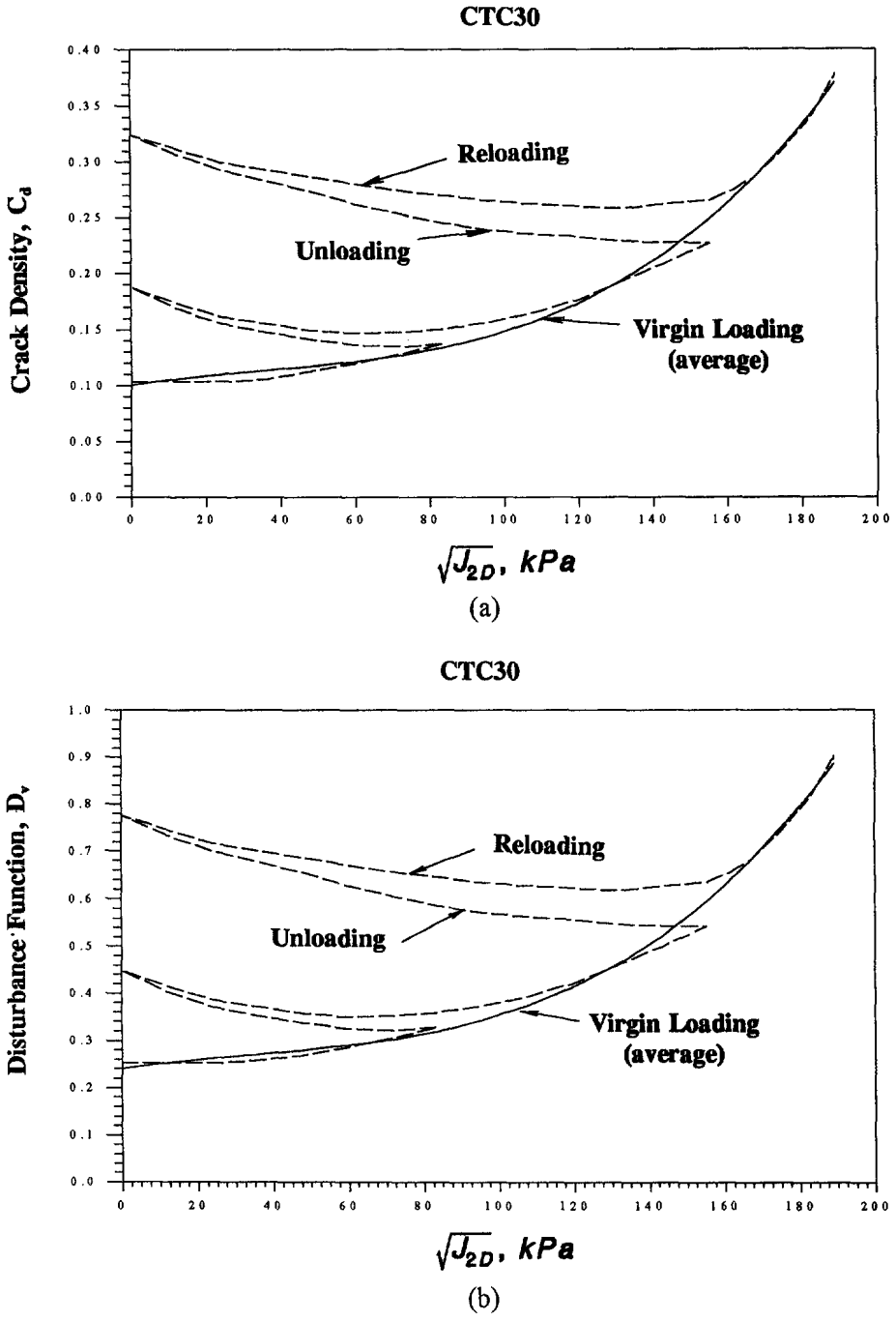

Fig. 12. Variations of D_v and C_d for CTC 30-cemented sand: (a) $\sqrt{J_{2D}}$ vs C_d; (b) $\sqrt{J_{2D}}$ vs D_v.

Figures 13(a) and (b) show C_d vs $\sqrt{J_{2D}}$ and D_v vs $\sqrt{J_{2D}}$ for the fiber ceramic. Here, $\sqrt{J_{2D}} = \sigma_1/\sqrt{3}$ as the tensile loading is uniaxial. Both C_d and D_v increase during the virgin loading. During unloading, they decrease because as the tensile stress is removed, the cracks would close. Then, during reloading and subsequent virgin loading, they increase.

Figure 14(a) and (b) shows plots of D_v vs C_d for tests on the cemented sand under different stress paths, and for the four tests on the ceramic, respectively. Based on these

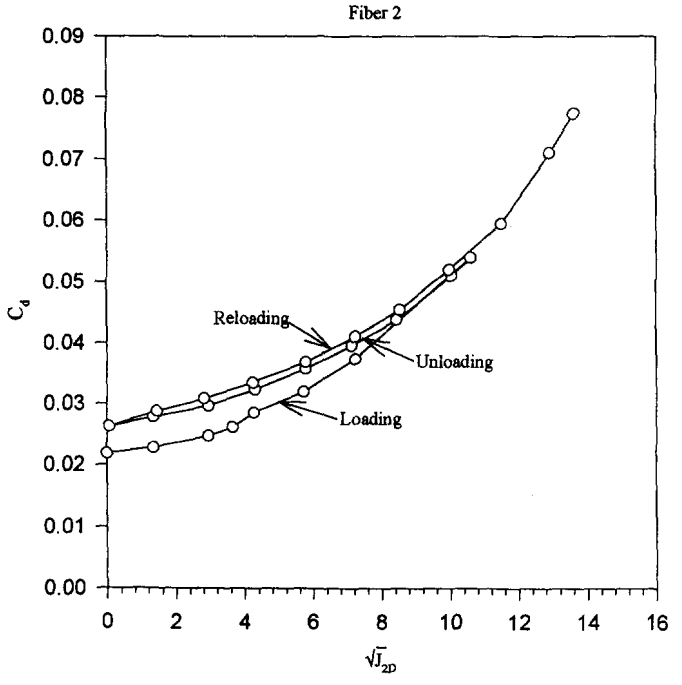

(a)

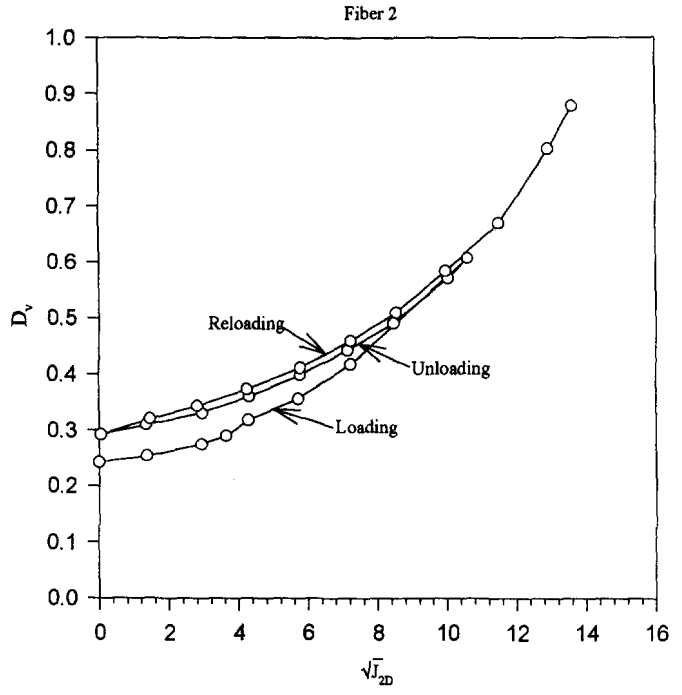

(b)

Fig. 13. Variations of D_v and C_d for fiber ceramic: (a) $\sqrt{J_{2D}}$ vs C_d; (b) $\sqrt{J_{2D}}$ vs D_v.

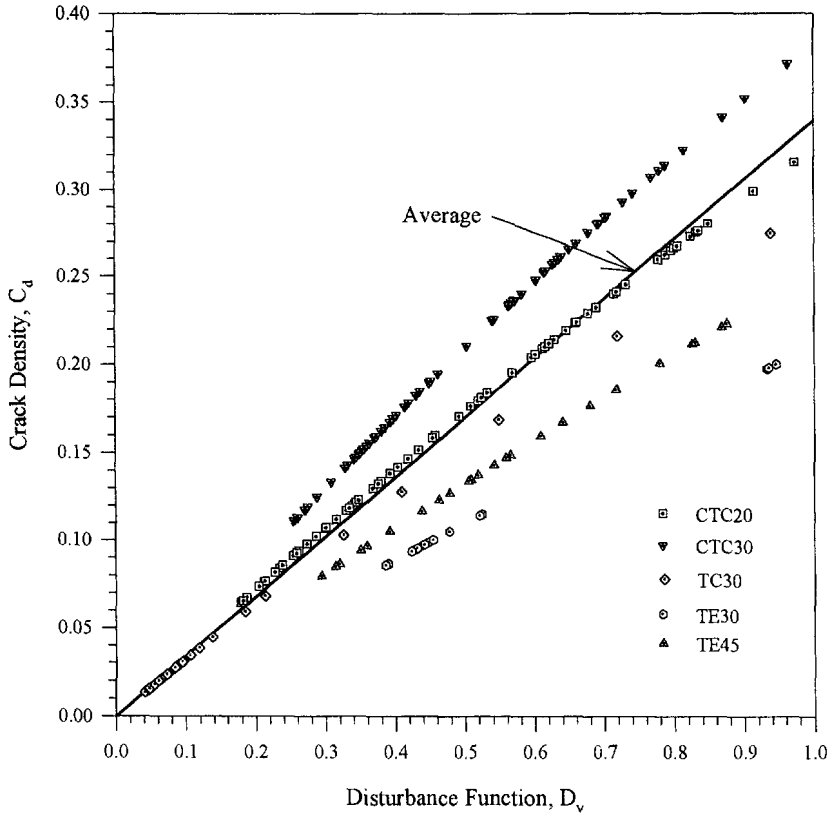

(a)

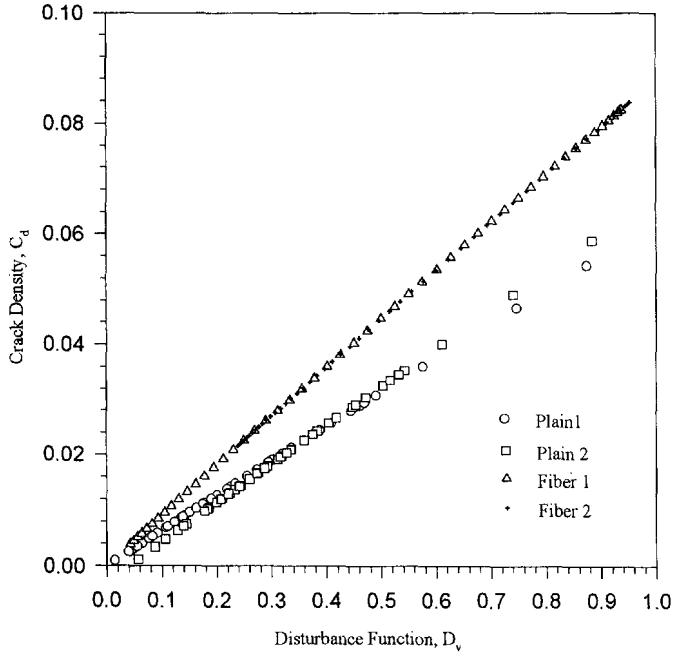

(b)

Fig. 14. Relation between C_d and D_t: (a) cemented sand; (b) ceramic.

results, approximate linear relations appear to exist between C_d and D_v. Thus, the crack density can be evaluated from the disturbance function, D_v.

8. CONCLUSIONS

The proposed disturbed state concept can allow unified characterization of the mechanical response of engineering materials. Since it is based on the modelling of the observed response in terms of interacting mechanisms involving the RI and FA states as the consequence of internal microstructural changes due to natural self-adjustment, the approach provides a fundamental model and can possess a number of advantages compared to other available models such as continuum damage, micromechanics and nonlocal enhancements of continuum models (Appendix 1). Various aspects of the model are investigated with respect to test behavior of two materials, a cemented sand and a ceramic, and are validated by comparing predictions with the test behavior.

It is shown that the disturbance function D can be defined based on both the stress–strain response and ultrasonic velocity measurements. The latter can provide simpler testing procedures and reduce the need for elaborate stress–strain testing. In addition to the characterization for the entire pre and post peak behavior, including effects of elastic and plastic strains, stress paths, microcracking, damage and softening, the approach can also be used to evaluate crack density and to define constitutive equations and moduli for predicting the remaining life of materials. The latter can have significant potential for design for the rehabilitation of existing structures. Thus, a fundamental and unified modeling approach can be *simplified* systematically for practical applications.

Acknowledgement—Parts of the research presented herein were performed under grant nos CES 8711764, CMS 9115316 and DDM 9102177 supported by the National Science Foundation, Washington, DC. Participation of Dr S. V. Jagannath for the test results on the cemented sand, of Drs G. Frantziskonis and F. F. Tang toward the development of the ultrasonic device with MTS testing (Fig. 4), and of Mr C. Basaran in the analysis and computer implementation of the DSC are acknowledged. Useful comments and criticisms from Dr H. B. Mühlhaus and Dr R. de Borst are highly appreciated.

REFERENCES

Aifantis, E. C. (1989). Plasticity and self-organization. In *Proc. Advances in Constitutive Laws for Engineering Materials* (eds F. Jinghhang and S. Murikami) International Academic Publishers, Oxford.

Armaleh, S. H. and Desai, C. S. (1994). Modelling and testing of a cohesionless material using the disturbed state concept. *Int. J. Mech. Behavior of Materials* **5,** 279–295.

Bak, P. and Chen, K. (1991). Self-organized criticality. *Scientific American*, January, 26–32.

Bak, P. and Tang, C. (1989). Earthquakes as a self-organized critical phenomenon. *J. Geophys. Res.* **94,** 15635–15637.

Basaran, C. and Desai, C. S. (1994). Implementation of disturbed state concept for thermomechanical behavior of electronic packaging problems. Report to NSF, Dept of Civil Engineering and Engineering Mechanics, University of Arizona, Tucson, Ariz.

Bazant, Z. P. (1994). Nonlocal damage theory based on micromechanics of crack interactions. *J. Engng Mech.*, ASCE **120,** 593–617.

Bazant, Z. P. and Lin, F. B. (1988). Nonlocal yield limit degradation. *Int. J. Numer. Meth. Engng* **26,** 1805–1823.

Chia, J. and Desai, C. S. (1994). Unified constitutive modelling of interfaces and solids in semiconductor devices. Report to NSF, Dept. of Civil Engng. and Engng. Mechanics, University of Arizona, Tucson, Ariz.

de Borst, R. and Sluys, L. J. (1991). Localization in a Cosserat continuum under static and dynamic loading conditions. *Comput. Methods Appl. Mech. Engng* **90,** 805–827.

Deresiewicz, H. (1958). Stress-strain reactions for a simple model of a granular medium. *J. Appl. Mech., ASME* **25,** 402–406.

Desai C. S. (1974). A consistent finite element technique for work-softening behavior. In *Proc. Int. Conf. on Comput. Methods in Nonlinear Mechanics* (eds J. T. Oden *et al.*) Univ of Texas, Austin.

Desai, C. S. (1987). Further on unified hierarchical models based on alternative correction on disturbance approach. Report, Dept of Civil Engineering and Engineering Mechanics, University of Arizona, Tucson, Ariz.

Desai, C. S. (1992). The disturbed state as transition through self-adjustment concept for modelling mechanical response of materials and interfaces. Report, Dept. of Civil Engineering and Engineering Mechanics, University of Arizona, Tucson, Ariz.

Desai, C. S. and Basaran, C. (1995). Mesh dependence in the disturbed state constitutive model. *Int. J. Numer. Meth. Engng*, submitted.

Desai, C. S. and Girdner, K. (1992). Structural materials from lunar simulants through thermal liquefaction. In *Proc. Engng Construction and Operations in Space II, ASCE*, Denver, Colo., pp. 528–536.

Desai, C. S., Jagannath, S. V. and Kundu, T. (1995). Mechanical and ultrasonic anisotropic response of soil. *J. Engng Mech., ASCE* **21,** 744–752.
Desai, C. S. and Ma, Y. (1992). Modelling of joints and interfaces using the disturbed state concept. *Int. J. Numer. Analyt. Meth. Geomech.* **16,** 623–653.
Desai, C. S., Shao, C. and Rigby, D. (1995). Discussion to evaluation of soil liquefaction by energy principles, by Figueroa *et al. J. Geotech. Engng, ASCE*, in press.
Desai, C. S., Somasundaram, S. and Frantziskonis, G. (1986). A hierarchical approach for constitutive modelling of geologic materials. *Int. J. Numer. Analyt. Meth. Geomech.* **10,** 225–257.
Desai, C. S. and Woo, L. (1993). Damage model and implementation in nonlinear dynamic problems. *Int. J. Computational Mech.* **11,** 189–206.
Figueroa, J. L., Saada, A. S., Liang, L. and Dahisaria, N. M. (1994). Evaluation of soil liquefaction by energy principles. *J. Geotech. Engng, ASCE* **120,** 1554–1569.
Frantziskonis, G. and Desai, C. S. (1987). Constitutive model with strain softening. *Int. J. Solids Structures* **23,** 751–767.
Hudson, A. (1981). Wave speed and attenuation of elastic waves in material containing cracks. *Geophys. J. Royal Astron. Soc.* **64,** 113–150.
Jagannath, S. V., Desai, C. S. and Kundu, T. (1991). Correlation between mechanical and ultrasonic responses for anisotropic behavior of soils under cyclic loading. Report to National Science Foundation, Dept of Civil Engineering and Engineering Mechanics, University of Arizona, Tucson, Ariz.
Kachanov, L. W. (1958). Time of rupture process under creep conditions (in Russian). *Izvestia Akedemii Nauk, USSR* **8,** 26–31.
Kachanov, L. M. (1986). *Introduction to Continuum Damage Mechanics*, Martinus Nijhoft Publishers, Dordrecht, The Netherlands.
Katti, D. R. and Desai, C. S. (1994). Modelling and testing of cohesive soil using the disturbed state concept. *J. Engng Mech., ASCE*, **121,** 648–658.
Krajcinovic, D. and Fonseka, G. V. (1981). The continuous damage theory of brittle materials. *J. Appl. Mech., ASME* **48,** 809–815.
Lemaitre, J. and Chaboche, J. L. (1985). *Mecanique des materiaux solides*. Dunod-Bordes, Paris.
Lewis, C. D. (1982). *Industrial and Business Forecasting Methods*. Butterworth Scientific, London, U.K.
Lubarda, V. A. and Krajcinovic, D. (1993). Damage tensors and the crack density distribution. *Int. J. Solids Struct.* **30,** 2859–2877.
Murakami, S. (1987). Arisotropic damage theory and its application to creep crack growth analysis. In *Proc. Second Int. Conf. on Constitutive Laws for Engng Materials* (eds C. S. Desai *et al.*), pp. 187–194. Elsevier, New York.
Mühlhaus, H. B. and Aifantis, E. C. (1991). A variational principle for gradient plasticity. *Int. J. Solids Struct.* **28,** 845–858.
Pijaudier-Cabot, G. and Bazant, Z. P. (1987). Nonlocal damage theory. *J. Engng Mech., ASCE* **113,** 1512–1533.
Roscoe, K. H., Schoefied, A. and Wroth, C. P. (1958). On yielding of soils. *Geotechnique* **8,** 22–53.
Sayers, C. M., van Munster, J. G. and King, M. S. (1990). Stress-induced ultrasonic anisotropy in berea sandstone. *Int. J. Rock Mech. Min. Sci.* **27,** 429–436.
Schreyer, H. and Chen, Z. (1986). One-dimensional softening with localization. *J. Appl. Mech., ASME* **53,** 791–797.
Tang, F., Desai, C. S. and Frantziskonis, G. (1992). Heterogeneity and degradation in brittle materials. *Engng Fract. Mech.* **43,** 779–796.
Toth, J. (1994). Development of linear ceramic composites, testing and constitutive modelling including cemented sand. Doctoral dissertation, Dept of Civil Engineering and Engineering Mechanics, University of Arizona, Tucson, Ariz.
Toth, J. and Desai, C. S. (1994). Development, testing and modelling of ceramic composites for lunar applications. In *Proc. Space* 94, *4th Int. Conf. on Engng Construction and Operations in Space, ASCE*, Albuquerque, N. M.
Van Mier, J. G. M. (1984). Strain softening of concrete under multiaxial loading conditions. Ph.D. dissertation, Eindhoven University of Technology, The Netherlands.
Vaid, Y. P. and Thomas, J. (1995). Liquefaction and post liquefaction behavior of sand. *J. Geotech. Engng, ASCE* **121,** 163–173.
Weibull, W. A. (1951). A statistical distribution function of wide acceptability. *Appl. Mech.* **18,** 293–297.
Yonenaga, I., Sumino, K. and Hoshi, K. (1984). Mechanical strength of silicon crystals as a function of the oxygen concentration. *J. Appl. Physics* **56,** 2346–2350.

APPENDIX 1

Various characteristics and comparison of the DSC with other models are presented below.

Thermodynamical consideration

Let the average or nonlocal strains and stresses over a representative dimension be denoted by $\{\varepsilon\}$ and $\{\sigma\}$, respectively. In the case of the finite element analysis, for instance, the area A_r of the material centered around (central) point, P, and enclosed by N integration points that participate in the averaging procedure can be treated as the representative dimension.

Now from the thermodynamical considerations, the material state can be characterized by its free energy density in the absence of thermal effects, which for the observed strains $\{\varepsilon^a\}$ and stress $\{\sigma^a\}$ is given by

$$\rho\psi^a = \tfrac{1}{2}\{\sigma^a\}^T\{\varepsilon^a\} \tag{A1-1}$$

where ρ is the mass density, and the stress is given by

$$\{\sigma^a\} = \frac{\partial(\rho\psi^a)}{\partial\{\varepsilon^a\}}. \tag{A1-2}$$

After substitution of eqn (2a) in eqn (A1-1) and differentiation with time of the resulting equation, the energy dissipation rate is given by

$$\varphi = \frac{\partial(\rho\psi^a)}{\partial t} = (\tfrac{1}{2}\{\varepsilon^a\}^T[C]^i\{\varepsilon^i\} - \tfrac{1}{2}\{\varepsilon^a\}^T[C^c]\{\varepsilon^c\})\dot{D}$$

$$= (\rho\psi^i - \rho\psi^c)\dot{D} \tag{A1-3}$$

where ψ^i and ψ^c are the free energies relevant to the RI and FA states, respectively. Now $\rho\psi^i$ and $\rho\psi^c$ are positive definite functions of mean strains, and from physical considerations $\rho\psi^i > \rho\psi^c$ because the energy in the RI state is greater than or equal to that in the FA state. Furthermore, $\dot{D}$ increases monotonically with time, hence, φ in eqn (A1-3) $\geqslant$ O, which satisfies the Clausius-Duhem inequality as per the Second Law of Thermodynamics. If $\{\varepsilon^a\} = \{\varepsilon^i\} = \{\varepsilon^c\}$ and $[C^c] = [0]$, implying that the material in the FA state does not carry any stress, eqn (A1-3) reduces to

$$\varphi = (\tfrac{1}{2}\{\varepsilon^i\}^T[C^i]\{\varepsilon^i\})\dot{D} \geqslant 0 \tag{A1-4}$$

which is the same as that in the previous nonlocal damage models, e.g. Pijaudier-Cabot and Bazant (1987).

Tangent stiffness matrix

Based on eqn (2) and evaluation of dD from eqn (7a), the incremental stress equations are given by [Basaran and Desai (1994)]

$$\mathrm{d}\sigma^a_{ij} = [(1-D)C^i_{ijkl} + D(1+\alpha)C^c_{ijkl} + (\sigma^c_{ij} - \sigma^i_{ij})R_{kl}]\,\mathrm{d}\varepsilon^i_{kl} \tag{A1-5a}$$

where $\mathrm{d}D = R_{st}\,\mathrm{d}\varepsilon^i_{st}$ and α is assumed to be given by

$$\mathrm{d}\varepsilon^c_{ij} = (1+\alpha)\,\mathrm{d}\varepsilon^i_{ij},$$

denoting relative strains between the RI and FA states. Now, eqn (A1-5a) can be written as

$$\mathrm{d}\sigma^a_{ij} = C^{DSC}_{ijkl}\,\mathrm{d}\varepsilon^i_{kl} \tag{A1-5b}$$

where C^{DSC}_{ijkl} is the overall disturbed state tangent constitutive tensor, which may not be positive definite, particularly in the softening region.

To analyze the characteristics of C^{DSC}_{ijkl}, a simple tension loading on a concrete bar, Fig. A1(a), is considered. The bar is 20 cm long, 10 cm wide and 1 cm thick. The concrete has properties the same as those determined from multiaxial tests reported by van Mier (1984); details of these parameters are given elsewhere [Basaran and Desai (1994), Desai and Woo (1993)].

Figure A1(a) shows the relative intact and observed (computed) behavior simulated by applying increments of strain in the finite element analysis. Figure A1(b) shows plots of various terms in eqn (A1-5a) normalized with respect to the initial tangent modulus vs average axial strain. It can be seen that the term $(1-D)C^i_{ijkl}$, which represents elastoplastic RI behavior, is always positive. On the other hand, the plot of C^{DSC}_{ijkl} shows that its value becomes negative around the peak strain of about $\varepsilon = 0.018$, and becomes positive after the strain of about $\varepsilon = 0.07$, which denotes the end of the softening zone and the initiation of the residual condition. The positive nature of C^{DSC}_{ijkl} after $\varepsilon = 0.07$, Fig. A1(b), is due to the fact that, in the proposed model with the value of $D_u = 0.875$ (for the concrete), there is always a positive value yielded by the first term in eqn (A1-5a).

Figure A1(b) also shows the variation of term $R_{kl}(\sigma^c_{ij} - \sigma^i_{ij})$, eqn (A1-5a), which contributes to the negative values of C^{DSC}_{ijkl}.

Since the finite element analysis involves strain-controlled loading, the solution converges in the softening zone by yielding decrease in stress under increasing applied strain. Under stress-controlled loading, the iterative procedures [Basaran and Desai (1994)] are based on computed strains; as a result, the solution also converges satisfactorily.

It is possible to use a simpler procedure in which the term $(\sigma^c_{ij} - \sigma^i_{ij})R_{kl}$ is evaluated at the previous step in the incremental procedure, and taken to the right-hand side as a load vector in the finite element equations. This does not mean that the basic nature of the problem is changed; however, such a procedure would involve a positive definite stiffness matrix corresponding to the first two terms in eqn (A1-5a), which are always positive.

Comparison with other models

Over the last two decades or so, the author and coworkers have been involved in research in the areas of constitutive modeling, laboratory and field testing, and implementation of the models in computational procedures. This research has included analysis and use of models based on such theories as nonlinear elasticity, plasticity and thermoviscoplasticity, and on fracture and continuum damage concepts. The concepts of self-adjustment or organization of deforming materials and the critical state soil mechanics have been considered towards unified interpretation of material response. Development of the DSC herein is an outcome of these efforts, which have benefited from the foregoing and available concepts. Thus, all ideas used in the DSC are not new. What can be considered different is the generalized interpretation of material behavior and the integration of some of the previous ideas to lead to a new and unified approach that permits characterization of a wide range of materials in

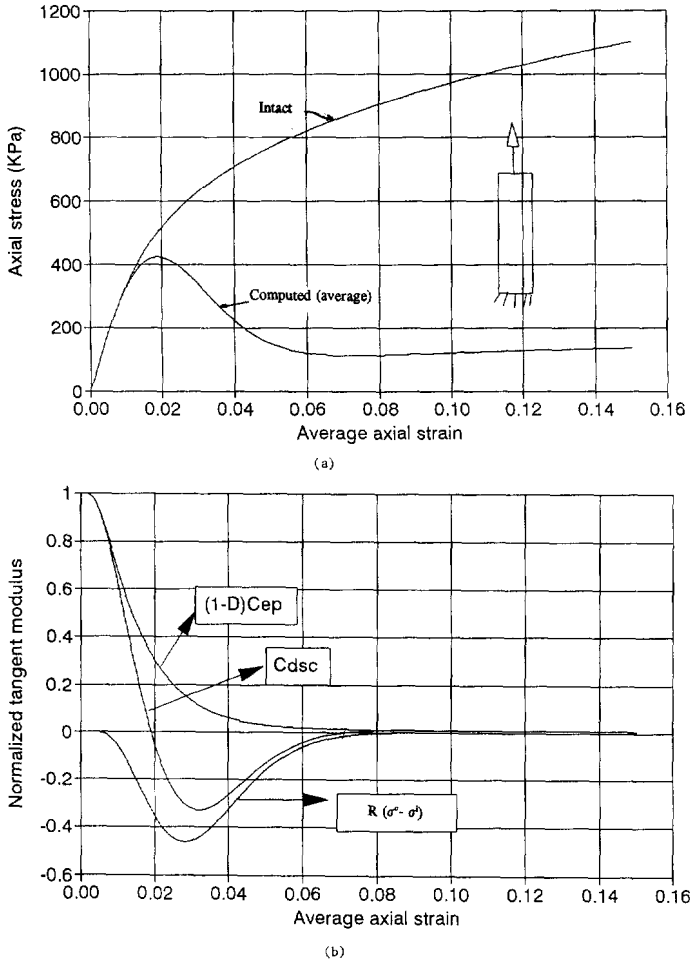

Fig. A1. Finite element results for one-dimensional tension test: (a) stress–strain; (b) tangent modulus vs axial strain.

a hierarchical manner. Some of the similarities and differences between the DSC and previous concepts such as the continuum damage, damage with microcrack interaction, micromechanics and self-organized criticality, and the advantages leading to the generalization in the DSC are discussed below.

The RI and FA stated in the DSC are analogous to the uncracked (undamaged) and cracked (damaged) parts in the damage models. In fact, the DSC can be considered to be a general concept in which the uncracked and cracked parts may be treated as special cases of the RI and FA states. Thus, the FA part in the DSC is treated as a modified material rather than just a cracked or damage part, and possesses specific stress–strain and strength properties during the deformation process.

The disturbance function, D, in the DSC and the damage parameter (ω) in the damage theory, eqn 3(b), are also similar. However, use of such a function is not unique in the DSC or in the damage theory because many natural growth and decay phenomena are described by using such a function. A difference is that, in the DSC, D can represent both growth (strengthening) and decay or softening (damage) processes, while the damage parameter usually represents deterioration or softening. Hence, the general term disturbance due to microstructural changes is used to cover both situations. For instance, behavior of materials such as loose granular and soft saturated clays that experience continuing compaction, and as a result stiffen, as well as those such as dense granular, rock and concrete that experience dilation, microcracking, damage and softening, can be included under the term disturbance.

Furthermore, use of the generalized term disturbance allows consideration of materials that may strengthen (after softening), during which the disturbance *decreases*; the traditional term, *damage*, would not be appropriate for these materials. Some examples of such materials are (1) silicon crystals doped by impurities such as oxygen [Yonenaga *et al.* (1984)], and (2) saturated sands at certain (loose) initial densities in the post liquefaction zones [Vaid and Thomas (1995)]. Applications of the DSC for these materials are in progress.

In the classical damage model, the cracked or damaged part of the material is assumed to be like a "void" [Kachanov (1958, 1986)], which possesses no strength. In subsequent works, the concept is extended to incorporate various factors such as creep, nonlocality, and the influence of cracks (at the micro level) by considering crack interactions [Krajcinovic and Fonseka (1981), Lemaitre and Chaboche (1985), Schreyer and Chen (1986), Murakami (1987), Bazant and Lin (1988), Bazant (1994)]. The nonlocal effects are introduced by defining mean or average variables (e.g. strains and stresses) over a representative dimension. The crack interactions are incorporated by superimposing the effects (stresses or forces) in one or multiple cracks on the conventional damage model. For instance, in a number of recent papers by Bazant and coworkers, e.g. Bazant (1994), the effect

of stresses causing defreezing or unglueing and propagation of cracks is superimposed on stresses in the uncracked material, which is often assumed to be linear elastic. On the other hand, in the DSC, the strains and stresses with corresponding energy and interaction effects are introduced through the second and third terms in eqns (2b) and (2c). Thus, in the DSC, the stresses and strains affecting the FA states, including microcracking, occur implicitly in the model, and it is not necessary to identify cracks and define stresses in them separately.

In the above context, another difference between the DSC and the modified damage theories is that in the DSC, the FA material resulting from microstructural changes, including microcracking, is treated as an interacting "solid" material constrained by the material in the RI state. In other words, in the DSC, the emphasis is on the macrolevel characterization of the material response based on the *collective behavior of interacting mechanisms* in "solid" materials in the RI and FA states, which are treated as parts of the mixture.

There is a conceptual difference between the DSC and the (modified) damage theories in that DSC involves a holistic or unified representation of the behavior material as a mixture of interacting components, rather than through superposition of interaction through independently defined responses of particles or cracks. Thus, a philosophical difference between the DSC and damage concept lies in the interpretation of material response. In the continuum damage concept, the cracked or damage part contributes to the degradation or loss in strength. On the other hand, the DSC relies on the idea that the material deforms as a mixture of interacting RI and FA states, and experiences microstructural changes that can lead to degradation or strengthening in the response.

Furthermore, the DSC allows characterization of the constitutive behavior of the materials in the RI and FA states based on laboratory tests at the macrolevel on finite-sized specimens. For instance, the RI response is defined from loading–unloading–reloading data in the initial range of the stress–strain behavior, while the FA response is found from the post peak behavior near the ultimate conditions, Fig. 2. This is considered to be an advantage compared to micromechanics and nonlocal damage models based on micromechanical considerations [Deresiewicz (1958), Bazant (1994)]. This is because, at this time, it is difficult to define constitutive equations and parameters for the particle and crack level microbehavior, which is required in these models. Hence, very often, the macrolevel measurements on finite-sized specimens are used to define the microbehavior, which appears to be a contradiction!

The particle level behavior, e.g. definition of the micro level constitutive behavior through relative tangential and normal responses between particles, as is done in many micromechanics models, is not included in the DSC. However, the relative motions between the RI and FA provides for the micro level responses, particularly when the size of the material (finite) element becomes smaller. Also, it is possible to define (approximately), based on the directional components of D (or C_d), the microcracking and its directions.

It is believed that the understanding of the behavior of complex material systems composed of millions and millions of particles may not be amenable to derivation from the understanding and definition of such individual components *separately*. This is partly because the response of such a complex *interactive* system is not proportional to the disturbance (stresses or forces) at the particle or microcrack levels, and because such a disordered and chaotic system does not yield to such traditional analysis [Bak and Tang (1989), Bak and Chen (1991)]. In the DSC, no such separation of the responses of individual components and global system is involved. In this sense, the DSC is similar to the recently proposed self-organized criticality (SOC) theory which is considered to be a holistic approach [Bak and Tang (1989) and Chen (1991)]. The basic idea in the SOC is "that dynamical (material) systems may self-organize into a critical state similar to that of systems undergoing continuous phase transitions". The main difference between the DSC and SOC is that the latter deals with catastrophic events such as earthquakes, collapse and avalanches, while the DSC intends to define the entire response of the material including pre and post peak behavior and collapse.

Mesh dependence

The DSC allows for relative motions such as translation and rotation between the (weighted) clusters of materials in the RI and FA states, yielding a diffusion type process, because of different stresses, $\boldsymbol{\sigma}^i$ and $\boldsymbol{\sigma}^c$, eqn 2(b), and strains $\boldsymbol{\varepsilon}^i$ and $\boldsymbol{\varepsilon}^c$, eqn 2(c), in the two states. The effective lever arm, d, Fig. A2, between $\boldsymbol{\sigma}^i$ and $\boldsymbol{\sigma}^c$, can be considered to relate to the internal dimension and provide the limiting mechanism for localization. Here, the ultimate disturbance D_u, which is mesh dependent, is related to the volume (area) fraction occupied by the FA material which composes the localization zone or shear band. Then, $D_u \simeq \mathbf{d}/L$, where L is the width of a finite element, and d is proportional to the thickness of the shear band. As a consequence, when the DSC model is implemented in a finite element procedure with averaging for strains and stresses over a characteristic dimension (e.g. area, A_e, enclosed by integration points in a finite element), the so-called *spurious* mesh dependence is reduced significantly or eliminated [Desai and Woo (1993), Desai and Basaran (1995)]. Thus, in the DSC, it is not necessary to introduce external enrichments as is done in the nonlocal, gradient and Cosserat models [Bazant and Lin (1988), de Borst and Sluys (1991), Mühlhaus and Aifantis (1991)].

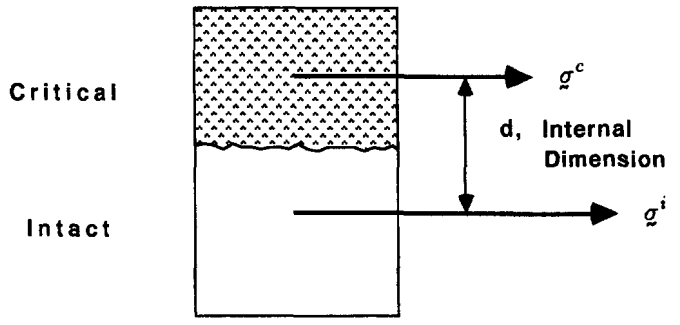

Fig. A2. Weighted materials in RI and FA (critical) states and relative motions.

In view of the above, the DSC is considered to provide a generalization and a number of capabilities beyond those provided by other concepts.

APPENDIX 2

The δ_0- version in the hierarchical single surface family of plasticity based models can be used to represent the RI state, Fig. 2(b). Here, the yield function F, which continuously expands in the stress space, is given by Desai *et al.* (1986),

$$F = \frac{J_{2D}}{P_a^2} - \left[\alpha\left(\frac{J_1}{p_a}\right)^n + \gamma\left(\frac{J_1}{p_a}\right)^2\right](1-\beta S_r)^{-0.5} = 0 \tag{A2-1}$$

where S_r is the stress ratio $J_{3D}^{1/3}/J_{2D}^{1/2}$, J_{3D} is the third invariant of S_{ij}, n, γ and are response parameters, and α is the hardening or growth function. n relates to the material state at which it transits from compaction to dilation, γ and are related to the ultimate envelope which is the locus of ultimate asymptotic stress states, and α is given by

$$\alpha = \frac{a_1}{\xi^{n_1}} \tag{A2-2}$$

where a_1 and η_1 are hardening parameters and $\xi = \int(d\varepsilon_{ij}^p\, d\varepsilon_{ij}^p)^{1/2}$ is the trajectory of total plastic strains and $d\varepsilon_{ij}^p$ is the plastic strain tensor. Use of the plasticity theory including the consistency and the consistency conditions, leads to incremental constitutive relation, eqn (4).

The values of the above parameters for the plasticity model (a_1, η_1, γ, and n) and the two elasticity moduli (E and ν), are found from laboratory stress–strain tests; details are given elsewhere [Desai *et al.* (1986), Jagannath *et al.* (1991), Toth (1994)].